

## Article

# Temperature Responsive Copolymers Films of Polyether and Bio-Based Polyamide Loaded with Imidazolium Ionic Liquids for Smart Packaging Applications

Daniela C. Zampino <sup>1</sup>, Gabriele Clarizia <sup>2,\*</sup> and Paola Bernardo <sup>2</sup><sup>1</sup> Institute of Polymers, Composites and Biomaterials (IPCB-CNR), Via P. Gaifami 18, 95126 Catania, Italy<sup>2</sup> Institute on Membrane Technology (ITM-CNR), Via P. Bucci 17/C, 87036 Rende, Italy

\* Correspondence: g.clarizia@itm.cnr.it

**Abstract:** Temperature-responsive materials are highly interesting for temperature-triggered applications such as drug delivery and smart packaging. Imidazolium Ionic Liquids (ILs), with a long side chain on the cation and a melting temperature of around 50 °C, were synthesized and loaded at moderate amounts (up to 20 wt%) within copolymers of polyether and a bio-based polyamide via solution casting. The resulting films were analyzed to assess their structural and thermal properties, and the gas permeation changes due to their temperature-responsive behavior. The splitting of FT-IR signals is evident, and, in the thermal analysis, a shift in the glass transition temperature ( $T_g$ ) for the soft block in the host matrix towards higher values upon the addition of both ILs is also observed. The composite films show a temperature-dependent permeation with a step change corresponding to the solid–liquid phase change in the ILs. Thus, the prepared polymer gel/ILs composite membranes provide the possibility of modulating the transport properties of the polymer matrix simply by playing with temperature. The permeation of all the investigated gases obeys an Arrhenius-type law. A specific permeation behavior, depending on the heating–cooling cycle sequence, can be observed for carbon dioxide. The obtained results indicate the potential interest of the developed nanocomposites as CO<sub>2</sub> valves for smart packaging applications.

**Keywords:** Imidazolium Ionic Liquids; temperature responsive materials; gas separation; polyether block amide



check for updates

**Citation:** Zampino, D.C.; Clarizia, G.; Bernardo, P. Temperature Responsive Copolymers Films of Polyether and Bio-Based Polyamide Loaded with Imidazolium Ionic Liquids for Smart Packaging Applications. *Polymers* **2023**, *15*, 1147. <https://doi.org/10.3390/polym15051147>

Academic Editor: Jason Bara

Received: 30 December 2022

Revised: 13 February 2023

Accepted: 22 February 2023

Published: 24 February 2023



**Copyright:** © 2023 by the authors. Licensee MDPI, Basel, Switzerland. This article is an open access article distributed under the terms and conditions of the Creative Commons Attribution (CC BY) license (<https://creativecommons.org/licenses/by/4.0/>).

## 1. Introduction

Smart polymeric materials, capable of reacting to small changes in the environment, are actively studied in the fields of nanoscience, nanotechnology and biomedical engineering for numerous applications [1]. Temperature-responsive polymers are of practical interest since their physical properties can be varied by changes in the external temperature [2]. As this is an easily measurable and controllable parameter, the thermal stimuli can be induced externally and thus in a non-invasive manner, as required in biomedical applications.

The loading of temperature-responsive materials into a polymeric matrix to prepare packaging systems is a strategy to regulate the permeation of gases or water vapor in response to temperature changes occurring on the external atmosphere. Among various temperature-responsive materials, Ionic Liquids (ILs) are salts with a low vapor pressure. By playing with the chemical structure of the ionic constituents, ILs can be solid at room conditions and thus can be adopted to induce a discontinuous thermal behavior in a polymer matrix, depending on their melting temperature. In particular, long-chain alkylimidazolium ILs (e.g., [C<sub>16</sub>MIM]Br and [C<sub>16</sub>MMIM]Br) have high heat capacity and high storage density [3].

Pebax<sup>®</sup> are block copolymers in which linear chains of hard polyamide (PA) are covalently linked to soft polyether (PE) blocks via ester groups [4]. The soft blocks, owing

to dipole–dipole interactions, are more flexible [4] and provide sustained gas permeability, while the hard PA segments guarantee mechanical stability. Different properties are available in these copolymers, depending on the PE and PA types and on their relative ratio. The biocompatibility enables the application of Pebax in the medical field (e.g., for virus-proof surgical sheeting or for short-term implants in humans) [5]. Flexible packaging is another application of these thermoplastic elastomers, as well as in selective separation of membranes. Indeed, sorption and permeation tests have evidenced the good affinity of the PE blocks in Pebax for the polar CO<sub>2</sub> gas molecules [6]. Accordingly, several studies have investigated the use of Pebax as membrane material, alone or including ILs [7–9], non-ionic surfactants [10,11], nanoparticles [12,13], or combined with both ILs and nanofillers [14,15].

In the present study, blends of the commercial copolymer Pebax<sup>®</sup>Rnew and two long-chain alkyimidazolium ILs ((HdmimDMSIP), with a C16 side chain on the Imidazolium ring in the cation and (OOMmimPF<sub>6</sub>) an ether C9 chain on the Imidazole-based cation), were developed as flexible films. Pebax<sup>®</sup>Rnew is based on Polyamide 11 (PA11), an aliphatic semi-crystalline homopolymer obtained from renewable raw materials. Its physical and mechanical properties (e.g., low water absorption, high tensile strength and stiffness) are mainly due to the hydrogen bonding between adjacent chains of the highly polar amide (–CONH–) groups [16]. Dense films were prepared by solution casting, immobilizing the synthesized IL salts within the polymer matrix, and using ethanol as solvent.

These novel Pebax/ILs composites as self-supported membranes were investigated regarding their structural and thermal properties, and the membranes were tested in gas separation, analyzing the effect of temperature on its potential applications in flexible packaging. Both of the selected ILs have a melting point of around 50 °C, thus, the prepared films were characterized in the same temperature range to study the effect of their solid–liquid transition on the permeation of gases. In particular, they have both an Imidazolium-based cation and Imidazolium ILs, which are more thermally stable than tetraalkyl ammonium-, piperidinium- and pyridinium-based ILs, independent of the anion [17]. The attractive features of these blends are represented by the use of a flexible and bio-derived thermoplastic copolymer of a green solvent [18], used for material processing and in thermally stable additives (Imidazolium ILs) that can display various phase change temperatures on the basis of the ionic constituents.

## 2. Experimental

### 2.1. Materials

1-methylimidazole, 1,3-dimethyl 5-sulfoisophthalate sodium salt, 1-bromohexadecane, chloromethyl octyl ether, sodium hexafluorophosphate, tetrahydrofuran, dichloromethane, hexane, ethyl acetate, dimethyl sulfoxide-d<sub>6</sub> and trans-2-[3-(4-tert-butylphenyl)-2-methyl-2-propenylidene]malononitrile, supplied by Sigma Aldrich (Milan, Italy), were used in the ILs synthesis. Ethanol absolute from VWR (Milan, Italy) was applied as a solvent in the membrane prepared. Chemicals were utilized as received.

The block copolymer Pebax<sup>®</sup>Rnew 25R53, based on a bio-polyamide 11 (PA11) and poly(tetramethylene oxide) (PTMO, in the range 79–83 wt% [19]), was received from Arkema (Milan, Italy).

Gases for permeation tests, including He, H<sub>2</sub>, O<sub>2</sub>, N<sub>2</sub> and CO<sub>2</sub>, were purchased with a purity of 99.99+% from SAPIO (Monza, Italy).

### 2.2. Methods

#### 2.2.1. IL Synthesis and Characterization

The structure of the ILs is reported in Figure 1. The synthesis of the ILs and their characterization by <sup>1</sup>H Nuclear Magnetic Resonance spectroscopy (<sup>1</sup>H NMR) and Matrix-Assisted Laser Desorption Time of Flight Mass Spectrometry (MALDI TOF MS) analyses was previously described [20,21]. Both ILs were synthesized according to a two-step method.

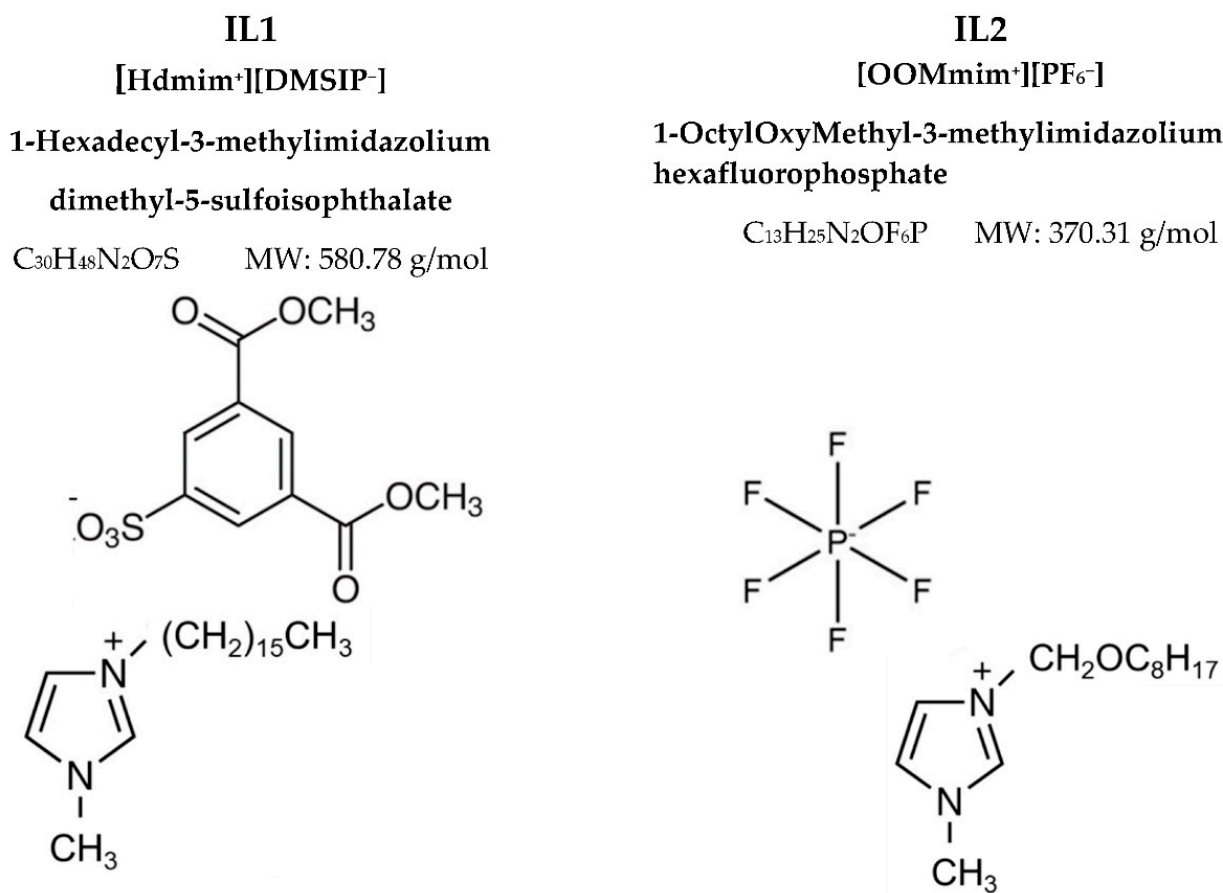


**Figure 1.** The chemical structures of the synthesized ILs.

*Synthesis of 1-hexadecyl-3-methylimidazolium dimethyl-5-sulfoisophthalate (HdmimDMSIP)*

The first step was the production of 1-hexadecyl-3-methylimidazolium bromide (HdmimBr) by reacting 1-bromohexadecane (6.4 mL, 20 mmol) with a solution of 1-methylimidazole (1.56 mL, 20 mmol) in 4 mL of ethyl acetate. The reaction was carried out at 65 °C under stirring in an inert nitrogen atmosphere for 24 h. The produced 1-hexadecyl-3-methylimidazolium bromide (HdmimBr) was cooled down to room temperature and filtered. A final washing with the ethyl acetate solvent enabled the removal of unreacted starting materials, leaving a white powder that was dried at 40 °C for 24 h in a vacuum oven (yield 95.6%).

The second step was a metathesis reaction between the HdmimBr (20 mmol, 7.77 g) in 40 mL of dichloromethane (DCM) and a solution of 1,3-dimethyl 5-sulfoisophthalate sodium (NaDMSIP, 20.9 mmol, 6.03 g) in water (130 mL). The two solutions were placed in a separating funnel and intensely shaken (30–45 min), reaching a condition in which two clear phases were separated without any precipitate. The organic layer was recovered, dried over magnesium sulfate and filtered. A Rotavapor removed the residual solvent. The HdmimDMSIP product was washed using ethyl acetate and dried for 24 h in a vacuum oven at 40 °C (yield 92.0%).

*Synthesis of 1-octyloxymethyl-3-methylimidazolium hexafluorophosphate (OOMmimPF<sub>6</sub>)*

The first step was the production of 1-octyloxymethyl-3-methylimidazolium chloride (OOMmimCl), which was obtained by stirring a mixture of chloromethyl octyl ether (3.86 mL, 0.02 mol) and 1-methylimidazole (1.585 mL, 0.02 mol) under nitrogen. The reaction was carried out for 30 min at room temperature. The obtained OOMmimCl was purified by repeating hot hexane (at 50 °C) washings and was recovered by filtration.

The second step was a metathesis reaction between a water solution (10 mL) of OOMmimCl (0.02 mol) and a water solution (10 mL) of sodium hexafluorophosphate (NaPF<sub>6</sub>, 0.02 mol). The two solutions were mixed, kept under stirring at 50 °C for 2 h, and

cooled down at room temperature. The organic fraction was recovered by centrifugation at 3000 rpm for 5 min. A final drying was carried out at 40 °C for 48 h, under vacuum (yield 95.0%).

The halide presence was monitored on the organic fraction, according to the Silver Nitrate Test. The complete exchange of the counter-ion was verified by analyzing aliquots of the organic fraction after the silver nitrate addition. The presence of a precipitate indicated that the exchange was not complete. For instance, in the case of the HdmimBr, this condition required that additional water solution, containing the NaDMSIP salt, was reacted with the organic layer to complete the anions exchange. Therefore, no residual halides were present in the produced ILs. Moreover, MALDI TOF analysis was an important tool not only to verify that the metathesis between the bromide/chloride synthesized with the chosen inorganic salts took place, but also to check the presence of halides (unreacted bromide/chloride) in the synthesized ILs. Indeed, no adduct peaks related to the presence of unreacted HdmimBr (expected peak at 695.76  $m/z$ ) and OOMmimCl (expected peak at 486.15  $m/z$ ) were found in the MALDI TOF spectra of the synthesized ILs.

On the contrary, the MALDI TOF analysis of ILs with very low yields showed peaks related to the simultaneous presence of the unreacted halides and the IL-synthesized adducts.

### 2.2.2. Membrane Preparation

The casting solution was prepared by dissolving the Pebax<sup>®</sup>Rnew pellets into ethanol at a concentration of 2 wt%. A clear solution was obtained under reflux conditions for ca. 2 h. Weighed amounts of ILs were added directly to the cooled polymer solution. The ILs were both solid at room temperature.

The membranes were prepared as dense flat sheets by casting the polymer/IL mixture within a stainless-steel ring placed onto a Teflon support. The ring was left at room conditions for a slow solvent evaporation. Isotropic films based on the neat polymer were also prepared and used as reference. The final membranes contained various IL concentrations (1, 5, 10 and 20 wt% of the total membrane weight).

### 2.2.3. Membrane Characterization

#### Fourier Transform Infrared (FT-IR)

Functional groups of the dense films were investigated by attenuated total reflection FT-IR analysis. The spectra were recorded in a FT-IR Spectrum One (Perkin Elmer, Milan, Italy), in the region of 4000 to 650  $\text{cm}^{-1}$ , with a resolution of 4  $\text{cm}^{-1}$  (16 scans). The same instrument was used in the transmission mode to analyze the neat ILs in the form of solid powders at room conditions by preparing KBr pellets in a hydraulic press.

#### Thermogravimetric Analysis (TGA)

Dynamic TGA curves were obtained under a nitrogen atmosphere at a purge flow of 60 mL/min using thermogravimetric equipment (Q500, TA Instruments, Milan, Italy). Samples (4–5 mg) were heated from 40 to 600 °C, at a heating rate of 10 °C/min.

#### Differential Scanning Calorimetry (DSC)

The melting and crystallization temperatures, as well as the glass transition temperatures, were measured by DSC, under a nitrogen flow, using a Q100 calorimeter (TA Instruments, Milan, Italy); this was supplied with a liquid sub-ambient accessory. The calorimetric measurements were performed in the temperature range of –90 to 200 °C, at a rate of 10 °C/min during both heating and cooling cycles. An empty aluminum pan and high purity standards (indium and cyclohexane) were used as reference and for calibration, respectively.

#### 2.2.4. Gas Permeation Tests

The tested samples had a circular effective area ranging from 11.3 to 2.14 cm<sup>2</sup>; their thickness was determined as the average of multiple point measurements taken by a digital micrometer (IP65, Mitutoyo). A fixed volume/pressure increase instrument (Elektro & Elektronik Service Reuter, Geesthacht, Germany) was used for the gas permeation tests with pure gases (H<sub>2</sub>, He, O<sub>2</sub>, N<sub>2</sub> and CO<sub>2</sub>) [22]. The feed pressure was 1 bar and the increasing gas pressure at the permeate side was monitored over time in a calibrated volume. The gas permeability ( $P$ ) was evaluated from the slope of the pressure vs. time curve:

$$p(t) = p(t=0) + \left. \frac{dp}{dt} \right|_{t=0} t + \frac{RTA}{V_p V_m} \frac{p_f P}{l} \left( t - \frac{l^2}{6D} \right) \quad (1)$$

where  $p_t$  is the permeate pressure at time  $t$ ,  $p_0$  is the starting pressure,  $(dp/dt)_0$  is the baseline slope,  $R$  is the universal gas constant,  $T$  is the absolute temperature,  $A$  is the exposed membrane area,  $V_p$  is the permeate volume,  $V_m$  is the molar volume of the permeating gas (at standard temperature and pressure, 0 °C and 1 atm),  $p_f$  is the feed pressure and  $l$  is the membrane thickness. The membrane samples were evacuated with a turbo molecular pump to remove previously dissolved species before each test. This step is particularly important also on fresh membrane samples, which can contain traces of residual solvent or gases adsorbed from the ambient. Indeed, ILs tend to pick up moisture from the environment and the water content of ILs has a crucial influence on their properties. Defect-free samples, that are well evacuated, have a negligible  $p(t=0) + \left. \frac{dp}{dt} \right|_{t=0}$  term.

The gas time lag ( $\theta$ ), obtained by extrapolating the transient linear portion of the pressure curve on the abscissa, is used to estimate the diffusion coefficient ( $D$ ) of each gas through the membrane [23]:

$$D = \frac{l^2}{6\theta} \quad (2)$$

The 'solution–diffusion' model that describes the transport in dense polymeric films [24] was considered to calculate the solubility coefficient ( $S$ ) as follows:

$$S = P/D \quad (3)$$

The ideal selectivity was obtained as the ratio of the specific permeability values for two gases. It can be decoupled into solubility selectivity and diffusion selectivity:

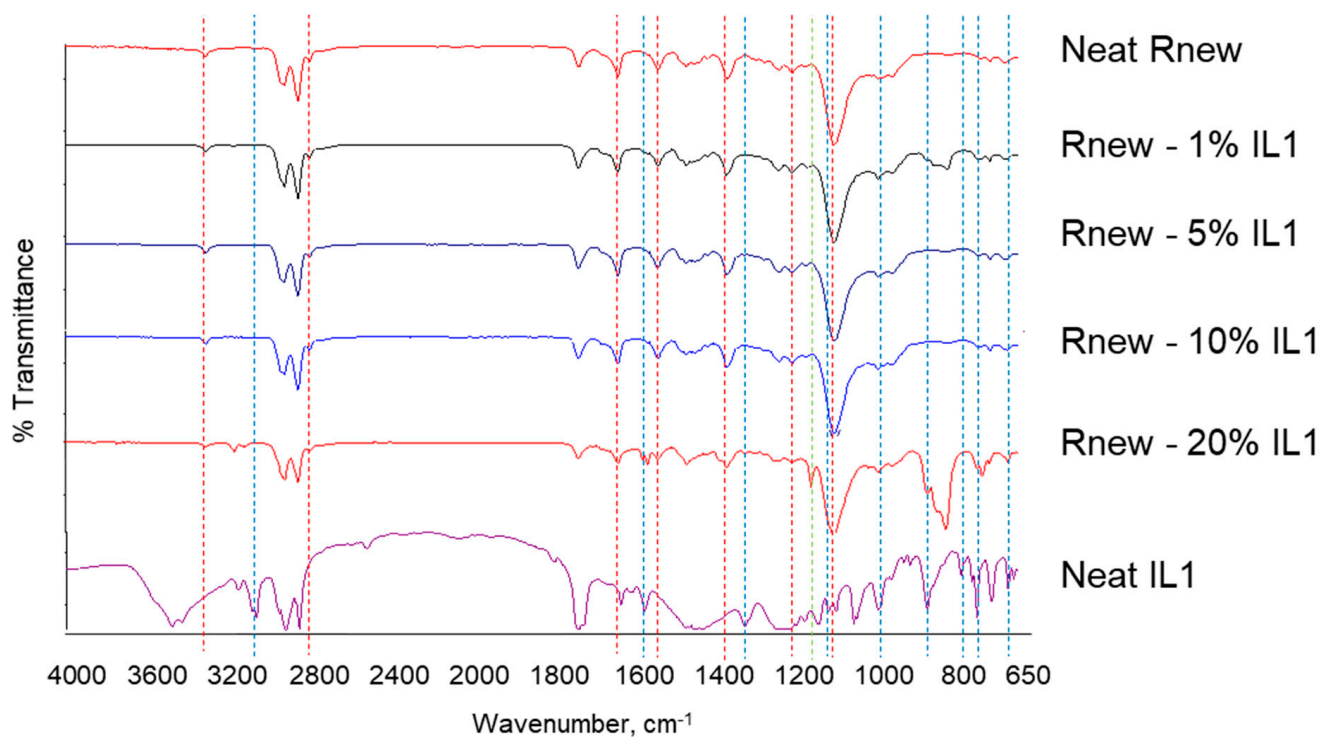
$$\alpha_{A/B} = P_A/P_B = S_A/S_B \times D_A/D_B \quad (4)$$

### 3. Results

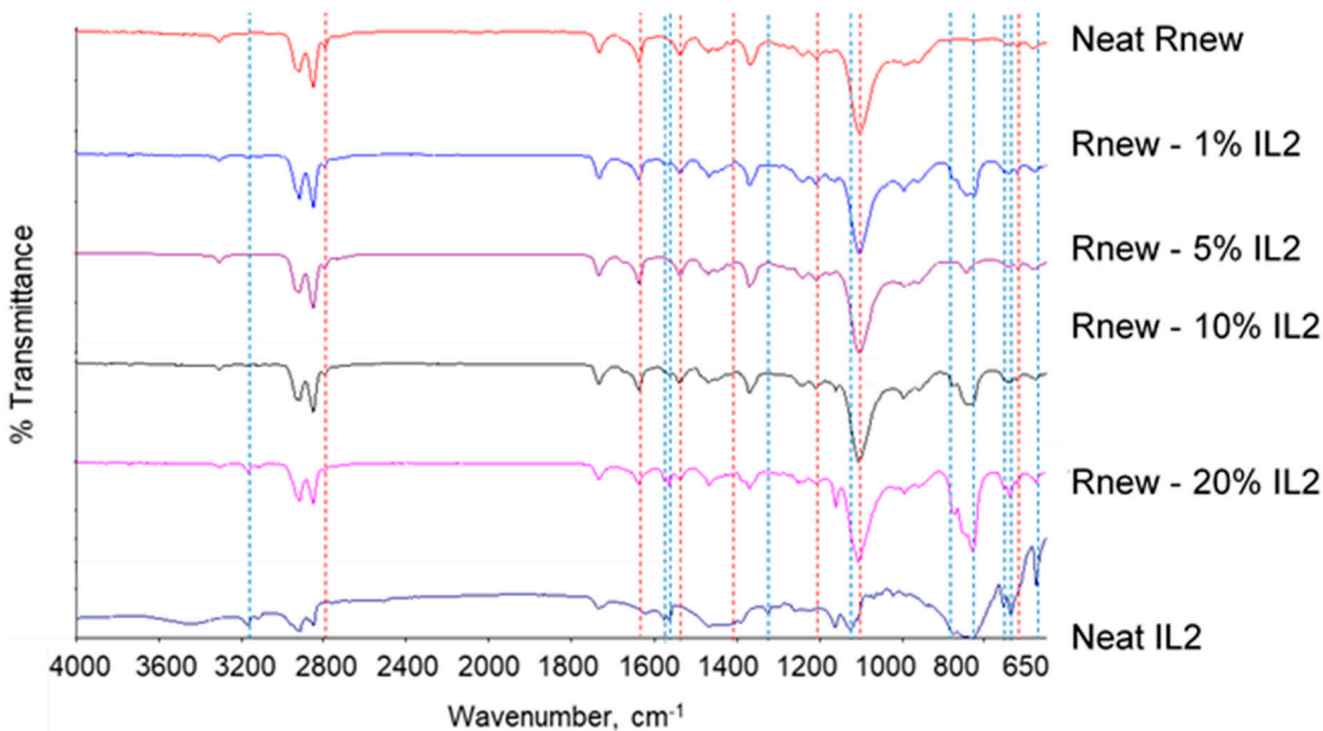
Both ILs were obtained as powdered materials at room temperature.

Homogeneous defect-free films were obtained with an average thickness of ca. 100 micron.

The synthesized ILs and the as-prepared film samples were analyzed by FT-IR and the obtained spectra are shown in Figure 2. The neat Pebax film displays strong bands at around 1100 and 1640 cm<sup>-1</sup>; these are related to the C–O–C (ether group) stretching vibrations within the PTMO block and to the H–N–C=O stretching vibrations in the polyamide, respectively. Another characteristic band for the pure Pebax<sup>®</sup> membrane is that which is assigned to the stretching vibrations of C=O at 1735 cm<sup>-1</sup> [25], while the peak at 3300 cm<sup>-1</sup> derives from the N–H stretching vibrations in the polyamide. The peaks at 2921 cm<sup>-1</sup> and 2852 cm<sup>-1</sup>, related to the aliphatic symmetric and asymmetric (C–H) stretching vibrations caused by the methyl groups in the polymer [25], are also characteristic of the selected ILs [26].



(A)



(B)

**Figure 2.** FT-IR spectra for Pebax®Rnew and Pebax®Rnew composite membranes. (A) Samples containing IL1 (HdmimDMSIP); (B) Samples containing IL2 (OOMmimPF<sub>6</sub>). Red dashed lines identify characteristic bands of the neat copolymer, while blue dashed lines identify characteristic bands of the neat ILs.

Both ILs present a  $\text{-C=N}$  stretching vibration band at around  $1635\text{ cm}^{-1}$  that is also distinctive of the polyamide block in the Pebax matrix.

The sulfone group in the anion of IL1 presents bands at  $1235\text{ cm}^{-1}$  (asymmetric vibration of  $\text{S=O}$ ) and around  $1060\text{ cm}^{-1}$  (symmetric vibration of  $\text{S=O}$ ), as shown in Figure 2A. The peak of  $830\text{ cm}^{-1}$  is a characteristic frequency of  $\text{PF}_6^-$ , while the band at ca.  $1130\text{ cm}^{-1}$  indicates the  $\text{C-O-C}$  ether stretching in the Imidazolium side chain (Figure 2B).

The composite samples, particularly in the fingerprint region, display characteristic peaks that are due to the Imidazole ring of the ILs. The band at  $1161\text{ cm}^{-1}$  is related to the Imidazole  $\text{H-C-C}$  and  $\text{H-C-N}$  bending and the band at  $752\text{ cm}^{-1}$  is characteristic of the out-of-plane  $\text{C-H}$  bending of Imidazole rings [27].

Physical interactions are evident in the nanocomposite films. The C atom between the highly electronegative neighboring two N atoms in the Imidazole ring of the IL cation can form hydrogen bonds [28]. The band characteristic of the in-plane Imidazole ring bending, which typically has a peak at  $840\text{ cm}^{-1}$  [27], is split into two bands (at  $828\text{ cm}^{-1}$  and  $855\text{ cm}^{-1}$ ) in the IL1 nanocomposites. They can be considered as hydrogen-bonded and free state (at higher wavelength), respectively, with a more intense bonded part. The same behavior is observable in both types of nanocomposites for the band at ca.  $1570\text{ cm}^{-1}$  (Imidazolium ring stretching [27]), which is split with intensity variations (at  $1564$  and  $1576\text{ cm}^{-1}$ ). Such splits can be attributed to specific interactions of the Imidazolium cation with the polymer matrix. In addition, the band for the out-of-plane  $\text{C-H}$  bending of the Imidazole ring has another peak at  $739\text{ cm}^{-1}$  due to the hydrogen-bonded state.

The polar PA block can form hydrogen bonds with smaller polar molecules [16]. The double peak, observed in the polymer matrix at  $1469\text{ cm}^{-1}$  and assigned to the  $\text{C=O}$  stretching vibration in carbonyl, has a more intense hydrogen-bonded part in the blends, indicating hydrogen bonding with the polyamide segments in Pebax. The peak at  $1538\text{ cm}^{-1}$  (bending of  $\text{N-H}$  in the PA block in Pebax [29]) is slightly blue-shifted at  $1541\text{ cm}^{-1}$  in both blends, revealing a bond contraction in the composite membranes. This indicates the high energy of these bonds in the polymer matrix.

As previously reported [20,21], the TGA thermograms, obtained during the dynamic degradation tests for both ILs, display a single degradation step, reaching the maximum temperature for decomposition at  $411\text{ }^\circ\text{C}$  (IL1) and at  $271\text{ }^\circ\text{C}$  (IL2). The decomposition onset temperature ( $T_{\text{onset}}$ ), a worthy descriptor of the thermal stability of a material, was  $340\text{ }^\circ\text{C}$  for IL1, whereas it was  $240\text{ }^\circ\text{C}$  for IL2, indicating a higher stability of IL1 than IL2; this is probably due to both the hygroscopicity of IL2 and the presence of an alkoxyated side chain in its Imidazolium cation [21].

The pristine Pebax®Rnew film and almost all its blends displayed a single degradation step, with no significant differences below  $200\text{ }^\circ\text{C}$ , indicating that the loading of the ILs does not affect the thermal stability of the polymer (Figure 3). Nevertheless, at temperatures above  $200\text{ }^\circ\text{C}$ , a decreasing trend in degradation temperatures was observed. In particular, the pristine polymer showed a  $T_{\text{onset}}$  at ca.  $366\text{ }^\circ\text{C}$  that shifted at lower temperatures according to the IL concentration in the blend films. Indeed, reductions of  $29\text{--}66\text{ }^\circ\text{C}$  and  $12\text{--}155\text{ }^\circ\text{C}$  were observed for the onset temperature in the films containing IL1 and IL2, respectively. The drastic decrease shown by the films containing  $5\text{--}20\%$  IL2 is probably due to absorbed water and residual solvent trapped in the polymer matrix, even after rigorous drying in a vacuum oven. This was confirmed by the peaks in the range  $210\text{--}230\text{ }^\circ\text{C}$ , evidenced in the DTG curves (Figure 4B).

The maximum degradation temperature ( $T_d$ ), as well as the temperature at a  $50\%$  weight loss in the blend films, showed a less pronounced decreasing behavior than the onset temperature, displaying reductions up to ca.  $50$  and  $10\text{ }^\circ\text{C}$  for the films containing  $20\%$  IL1 and IL2, respectively (Table 1).

The DTG curves highlight the shift for the peak corresponding to the polymeric matrix at lower temperatures (Figure 4). Typically, the decomposition temperature of the IL decreases for longer alkyl chains on the cation [30]. In our study, the Rnew-IL1 films showed a clear shift to lower temperatures, particularly evident for the  $20\%$  concentration,

whereas minor shifts were observed in the Rnew–IL2 blends. A shoulder, observed at ca. 390 °C (Rnew–20%IL1) and at 430 °C (Rnew–20%IL2), is indicative of a complexation between the polymer and the ILs [31]. This shoulder was more outlined in the sample containing 20% IL2. Moreover, the peaks detected at 210–230 °C (Rnew–5–20% IL2) are due to the hygroscopic behavior of IL2 and the solvent residue from film preparation, as mentioned above.

The residue of the polymer films is not different with respect to that of neat Pebax, except for the films containing an IL concentration of 20%. In these blends, a slight increase in the residue is observed, probably due to the complexes between the ILs and the polymer, which do not completely degrade up to 600 °C.

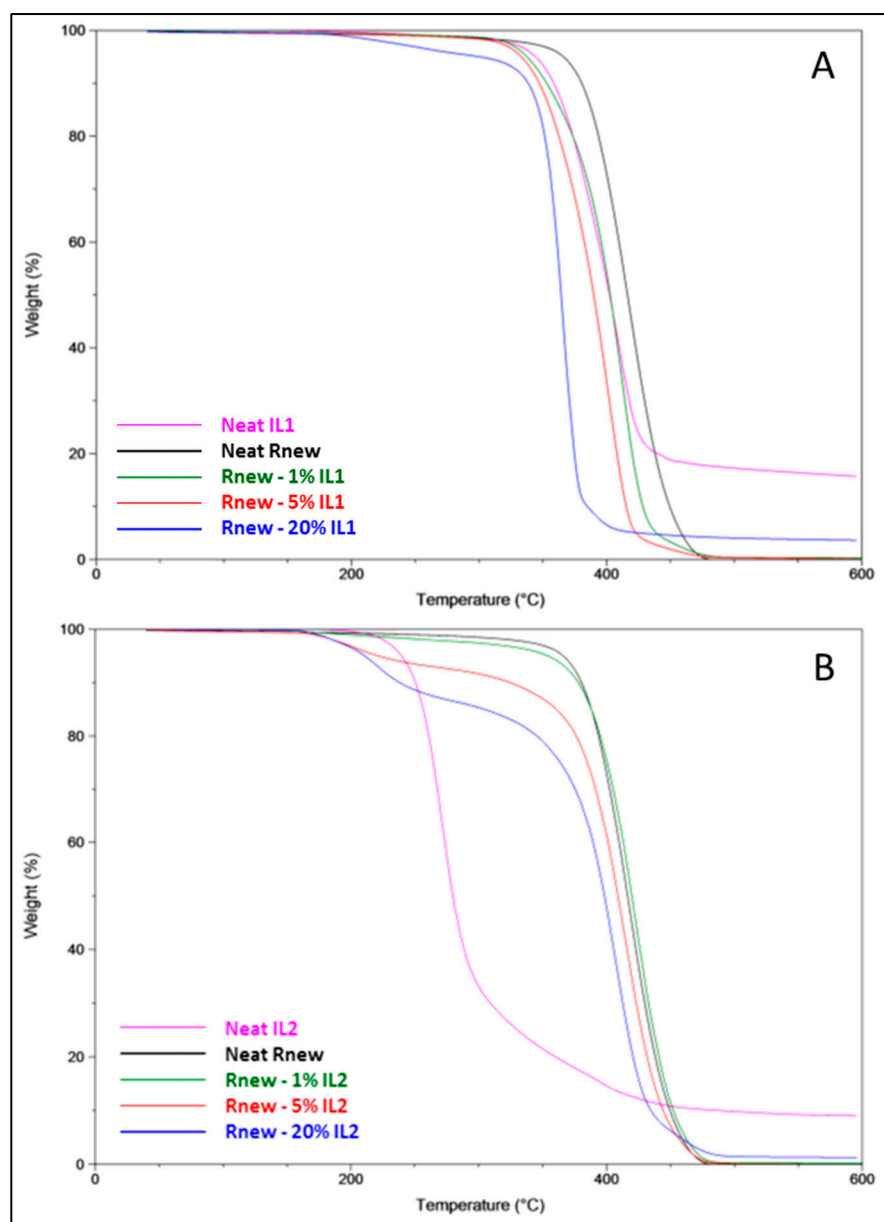


**Figure 3.** TGA thermograms for Pebax<sup>®</sup>Rnew and Pebax<sup>®</sup>Rnew composite membranes. (A) Samples containing IL1 (HdmimDMSIP); (B) Samples containing IL2 (OOMmimPF<sub>6</sub>).

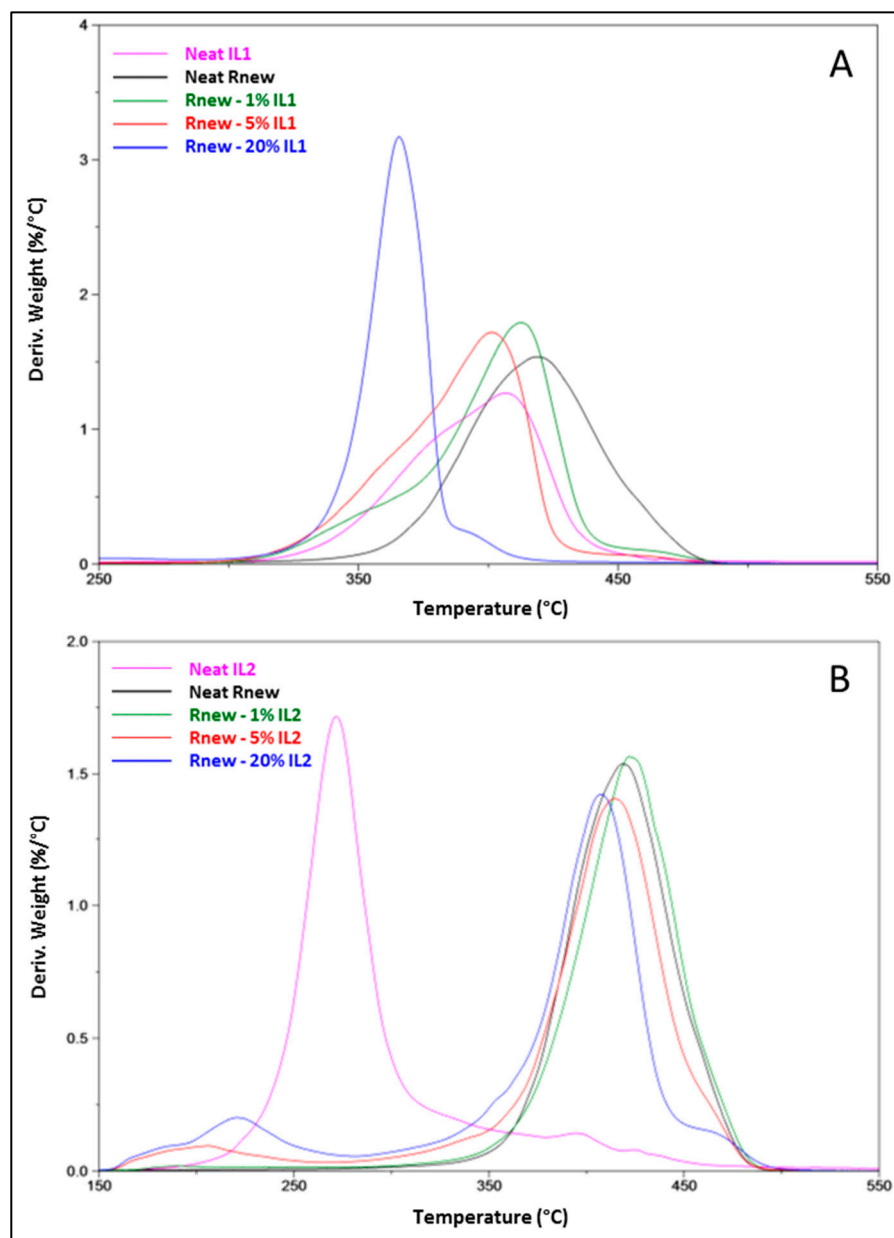


**Figure 4.** DTGA thermograms for Pebax<sup>®</sup>Rnew and Pebax<sup>®</sup>Rnew composite membranes. (A) Samples containing IL1 (HdmimDMSIP); (B) Samples containing IL2 (OOMmimPF<sub>6</sub>).

**Table 1.** Thermogravimetric data of neat Pebax<sup>®</sup>Rnew and its ILs blends.

Sample	T <sub>Δm = 5%</sub> (°C) <sup>a</sup>	T <sub>Δm = 50%</sub> (°C) <sup>b</sup>	T <sub>d1</sub> (°C) <sup>c</sup>	% R <sup>d</sup>
Neat Rnew	366	416	418	0.0
Rnew-1% IL1	337	403	413	0.2
Rnew-5% IL1	333	389	402	0.1
Rnew-20% IL1	300	364	366	3.6
Rnew-1% IL2	354	420	422	0.2
Rnew-5% IL2	222	409	415	0.0
Rnew-20% IL2	211	398	408	1.3

<sup>a</sup>: Onset of degradation (temperature of 5% weight loss); <sup>b</sup>: Onset of degradation (temperature of 50% weight loss); <sup>c</sup>: Decomposition maximum temperature of thermal degradation; <sup>d</sup>: Weight residue (%) at 600 °C.

The temperature ramp rate of 10 °C/min, used in the dynamic TGA under nitrogen, was the same as that adopted in the DSC analyses.

The DSC investigation on the neat ILs evidenced distinct melting points upon heating at ca. 49 °C and 52 °C for IL1 and IL2, respectively. Their freezing point was considerably lower, at −4 °C for IL1 and 7 °C for IL2 (Figure 5). No glass transition temperatures ( $T_g$ ) and no significant differences in IL melting ( $T_m$ ) and crystallization ( $T_c$ ) were found when comparing the first and second heating runs. However, IL1 displays a multifaceted phase behavior (Figure 5A) compared to IL2 (Figure 5B), as previously reported [20,21]. Indeed, in the second heating, a polymorphic behavior, characterized by cold crystallization and endothermic transitions, likely due to the melting of different crystals or solid-solid transitions, was found [20,21].

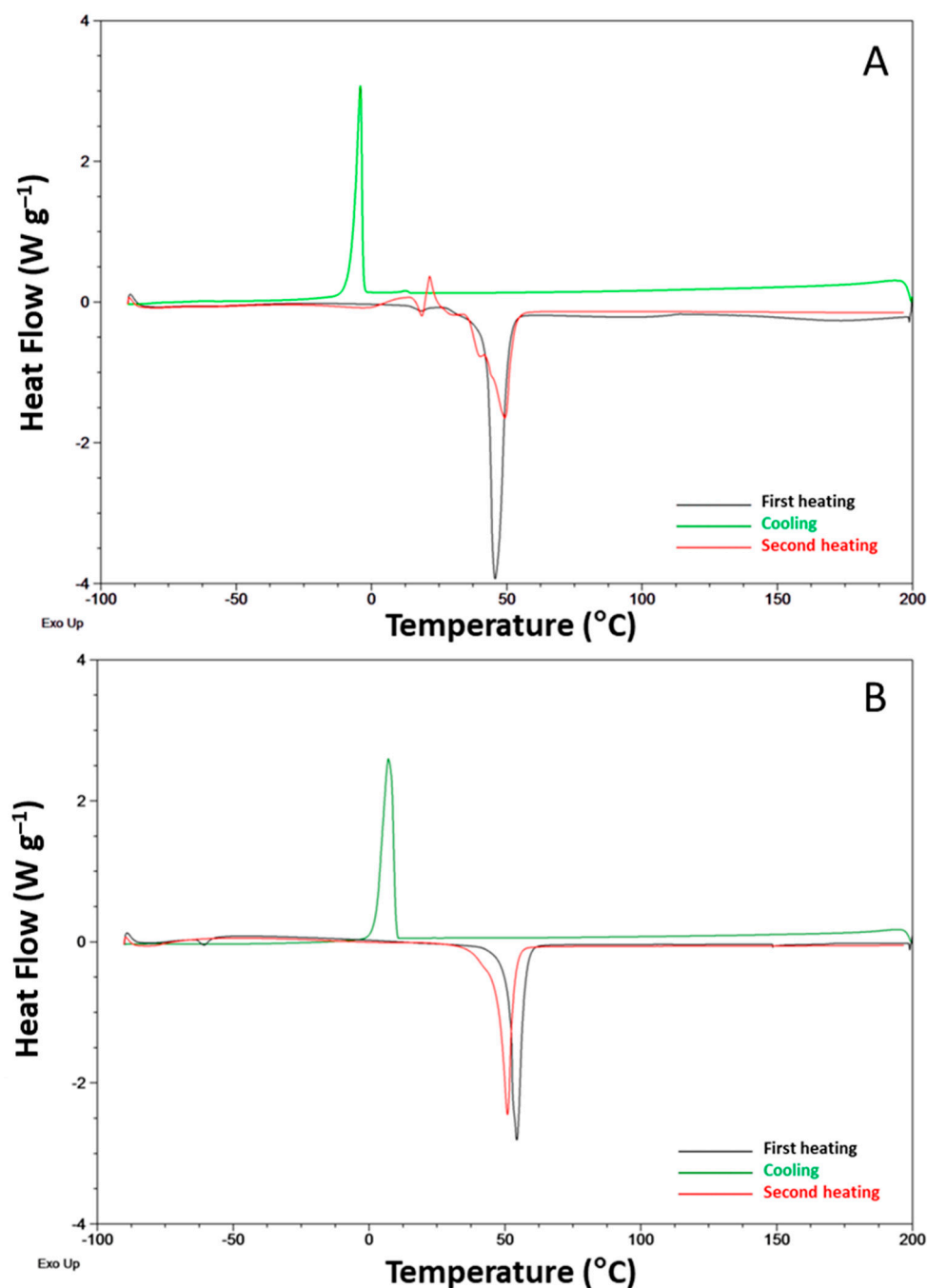
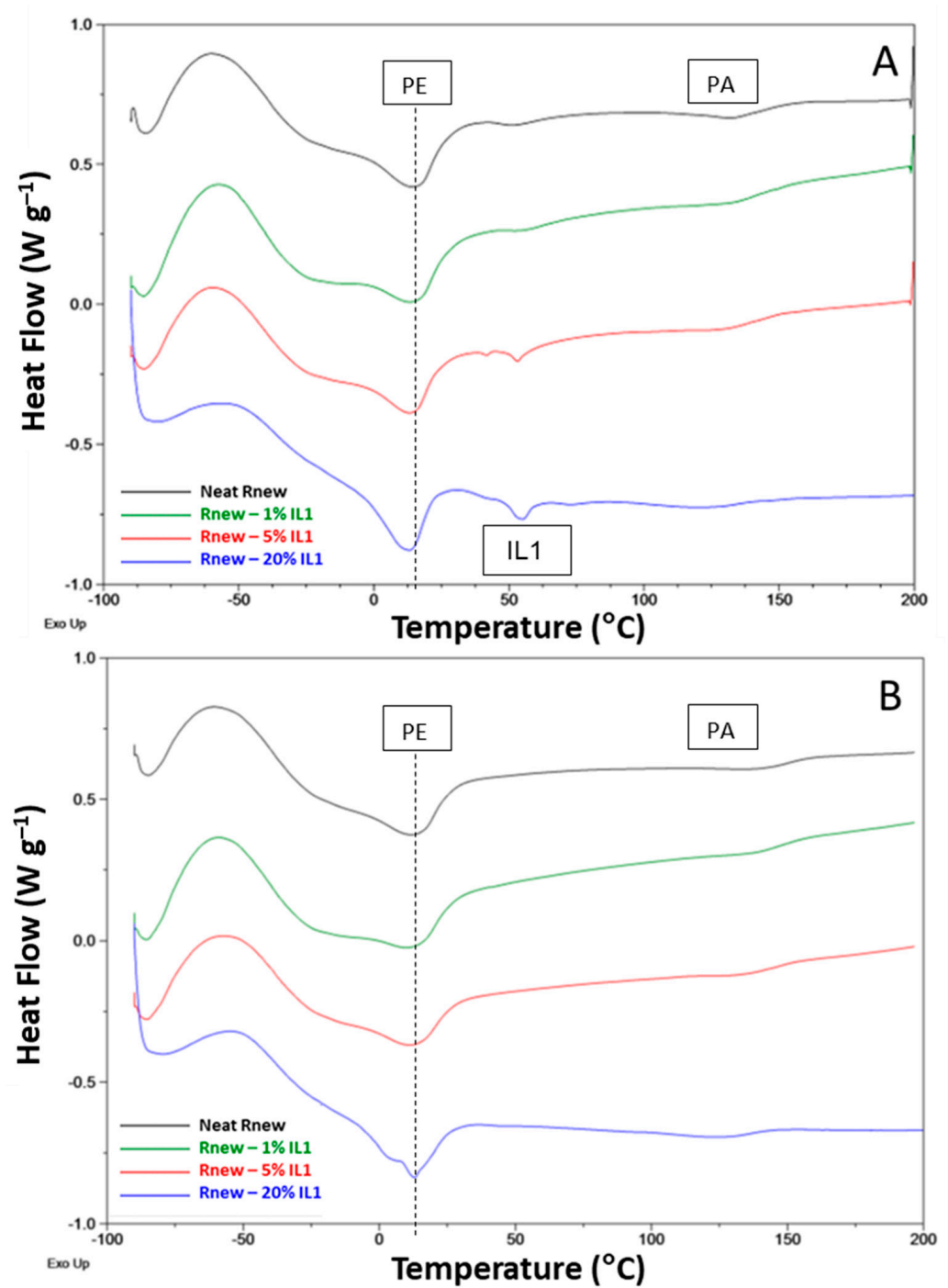
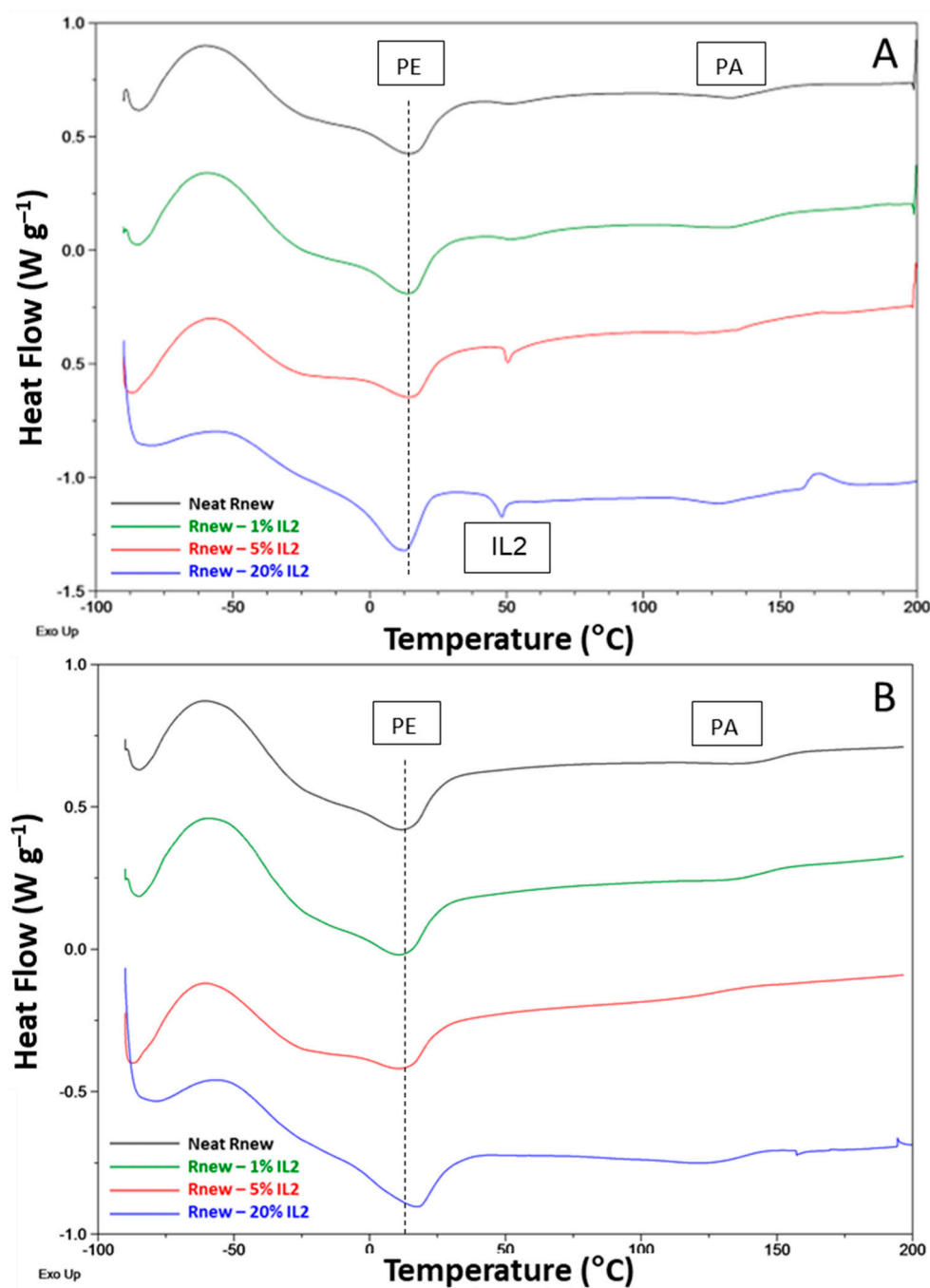


Figure 5. DSC traces for the neat ILs. (A) IL1 (HdmimDMSIP); (B) IL2 (OOMmimPF<sub>6</sub>).

As shown in Figures 6 and 7, the first heating scan for the neat Pebax membrane presents the melting peaks for the PA11 block and PTMO at ca. 140 °C and 13 °C, respectively. Indeed, the hard PA11 segment is reticulated by hydrogen bonding, resulting in a rigid crystalline block with a high melting temperature. The Pebax soft segment has a low  $T_g$ , of ca. -39 °C. This scan displays the behavior of the films prepared from the solution casting, which were not subjected to thermal cycles.



**Figure 6.** DSC traces for neat Pebax<sup>®</sup>Rnew and Pebax<sup>®</sup>Rnew-IL1 (HdmimDMSIP) composite membranes. (A) First heating scan; (B) Second heating scan.



**Figure 7.** DSC traces for neat Pebax<sup>®</sup>Rnew and Pebax<sup>®</sup>Rnew-IL2 (OOMmimPF<sub>6</sub>) composite membranes. (A) First heating scan; (B) Second heating scan.

In all samples, at ca. 60 °C, a broad peak was observed, probably due to a kinetically less favorable crystal phase induced by the slow solvent evaporation during membrane preparation. This peak and the melting peaks of both ILs loaded at high concentrations into the polymer matrix disappeared during the second heating run, suggesting that these crystalline phases form in the films from the solution state containing solid ILs, while a different behavior is found for the blends analyzed in the molten state. A slight shift to high temperatures (16 °C) for the  $T_m$  of the PTMO block and 144 °C for the PA block was observed.

Despite the different composition, the selected ILs display similar temperatures in their thermal transitions (see DSC analysis, melting temperature at ca. 50 °C), enabling their characterization in the same temperature range to study the effect of this solid-liquid

transition on the resulting gas permeation properties of the prepared films. The heat capacity ( $c_p$ ) of the two ILs was calculated on the basis of two correlations available in the open literature [32,33]. According to Ahmadi et al. [32], the  $c_p$  values calculated at 25 °C are 1114 and 587 J/(mol K) for IL1 and IL2, respectively. Similar values are obtained applying the correlation developed by Farahani et al. [33]: 1097 and 562 J/(mol K) for IL1 and IL2, respectively. These calculations well match the experimental data available for Imidazolium-based ILs, since by increasing the side alkyl chain in the cation and, in general, the molecular weight of the salt, the thermal capacity and also the viscosity increase.

Both ILs induce a reduced crystallinity for the predominant PTMO phase, as testified by the decrease in the associated melting enthalpy ( $\Delta H_m$ ), particularly in the films containing a higher concentration of ILs. Moreover, the PTMO has a melting point below room temperature; consequently, it is amorphous at higher temperatures.

Crystallization peaks are clearly visible at a reduced temperature in the cooling cycle (Figure 8) for the Pebax blocks (ca. 40 °C PA11 and −14 °C PTMO). These peaks shift to slightly higher temperatures, with a 2–4 °C increase for both blocks in the blend films.

In general, IL addition to Rnew did not influence the positions of the melting and crystallization peaks; the slight shifts (1–5 °C) detected suggest no interaction and, consequently, phase separation between the polymer and the ILs.

The characteristic peaks of the copolymer relative to the melting for the polyamide and polyether blocks are preserved in the composite films; however, the  $T_{\text{melting}}$  is only slightly influenced upon the IL addition.

In the blends, the  $T_g$  values of the PTMO segment showed an increase of 1–3 °C upon the loading of the ILs with respect to the pristine polymer, indicating a reduced mobility in the amorphous polymer block, particularly in the IL1 samples at a high concentration. As a consequence, the polymer's stiffness and chain mobility are affected. Indeed,  $T_g$  is a cohesive energy parameter [34]. Moreover, the ILs in the composite membranes have a phase transition ( $T_{\text{melting}}$ ) of 55 °C for IL1 and 48.1 °C for IL2 (first heating scan). The previous thermal history was removed by heating them to above their melting point. Considering the cooling scan, no crystallization peak related to the ILs was present in the nanocomposite films. Thus, no supercooling was evident for both ILs once incorporated in the membrane. Accordingly, no melting peaks can be observed for the IL phase in the second heating trace for both ILs. In the case of the Rnew–IL1 blend at 20%, the PTMO melting is anticipated, as evidenced by a shoulder on the melting peak at around 4 °C due to metastable crystals that melt before the more stable ones.

Therefore, the film formed via solvent casting, represented by the first heating trace, is different from that obtained from the molten state after the polymer heats up to a high temperature (ca. 200 °C) and cools at the rate of 10 °C/min.

The gas permeation tests provided the main transport parameters: permeability, diffusion, solubility and the ideal selectivity for each of them. The data measured at 25 °C on the as-prepared samples are reported in Table 2. The considered permanent gases, with a molecular size below 1 nm, act as molecular probes for the membrane microstructure. At a certain temperature, the gas permeability is indicative of the membrane morphology, the polymer structure (e.g., degree of crystallinity) and chemistry (e.g., ratio of the two blocks), as well as the polymer/permeant interactions.

The gas permeation data confirm the dense nature of all the prepared films. Due to the large amount of the flexible PTMO segments in the copolymer, Pebax®Rnew presents a sustained gas permeability [20]. Table 3 proposes a comparison with other Pebax® grades, showing a reduced gas permeability when the amount of the PE block is lowered. Indeed, the melting point for the crystalline part of the polyether block is below room temperature, as indicated by DSC. In the neat Pebax®, the predominant polyether block is responsible for a preferential affinity for CO<sub>2</sub>, compared to nonpolar gases such as N<sub>2</sub> and H<sub>2</sub> [35].

In the case of the composite membranes, the amount and type of the IL also affects the permeation parameters and the transport mechanisms (Table 2). At room temperature, the addition of increasing quantities of both ILs to Pebax® progressively decreased the

overall gas permeability. Therefore, the solid ILs acted as impermeable fillers that were incorporated in the polymer matrix. The permeation rates of the tested gases in the composite films follow the same order as in the neat polymer, with CO<sub>2</sub> being the most permeable species, as in the pristine polymer matrix (Table 2). On the other hand, CO<sub>2</sub> molecules can also favorably interact with the cationic Imidazolium  $\pi$  system in the added ILs [38]. The nature of the anion in Imidazolium-based ILs has a key role in determining the affinity with CO<sub>2</sub> [39,40]. Typically, ILs and PILs that comprise the PF<sub>6</sub> anion display a good CO<sub>2</sub> solubility [39]. In addition, the Sulfonic group in the DMSIP anion IL1 displays a strong affinity with CO<sub>2</sub> via specific dipole–dipole interactions [28,41].

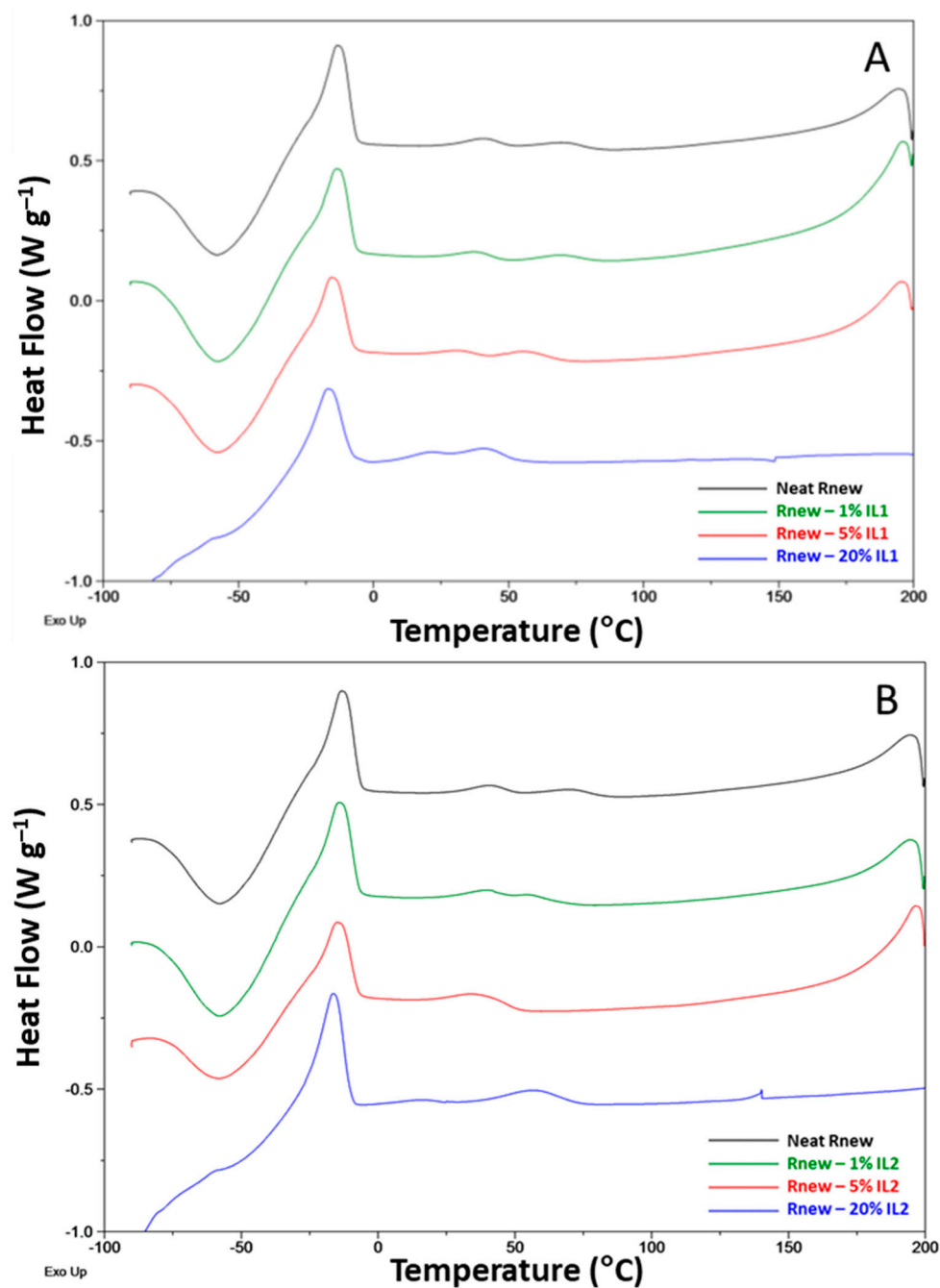


**Figure 8.** DSC traces for neat Pebax® Rnew and Pebax® Rnew composite membranes. Cooling scan. (A) Samples containing IL1 (HdmimDMSIP); (B) Samples containing IL2 (OOMmimPF<sub>6</sub>).

**Table 2.** Gas permeability measured on the as-prepared Pebax<sup>®</sup>Rnew and Pebax<sup>®</sup>Rnew/IL composite membranes at 25 °C.

Sample	Permeability (Barrer)					Selectivity (–)		
	CO <sub>2</sub>	O <sub>2</sub>	N <sub>2</sub>	He	H <sub>2</sub>	CO <sub>2</sub> /N <sub>2</sub>	H <sub>2</sub> /N <sub>2</sub>	O <sub>2</sub> /N <sub>2</sub>
Neat Rnew	247	23.6	8.9	25.7	45.4	27.9	5.12	2.66
Rnew–1% IL2	232	22.4	8.6	25.7	-	27.0	-	2.60
Rnew–5% IL2	226	21.6	8.1	23.8	38.1	28.0	4.73	2.61
Rnew–10% IL2	139	13.3	5.2	18.4	25.9	27.0	5.01	2.57
Rnew–20% IL2	117	11.5	4.1	17.4	25.1	28.3	6.14	2.77
Rnew–1% IL1	217	21.4	8.5	23.7	-	25.6	-	2.53
Rnew–5% IL1	195	19.2	7.2	24.1	40.3	27.2	5.63	2.68
Rnew–10% IL1	191	18.4	6.86	23.4	36.2	27.8	5.28	2.68
Rnew–20% IL1	98.4	10.4	4.4	13.4	23.2	22.3	5.25	2.35

1 Barrer = 10<sup>-10</sup> cm<sup>3</sup> (STP) cm cm<sup>-2</sup> cmHg<sup>-1</sup> s<sup>-1</sup>.

**Table 3.** Composite different Pebax<sup>®</sup> grades and gas permeability for measured in the corresponding membranes.

Grade	Composition	PE wt%	PA wt%	Permeability (Barrer)		Ref.
				CO <sub>2</sub>	T	
Neat Rnew	PTMO/PA11	79–83	17–21	247	25 °C	[This work]
2533	PTMO/PA12	80	20	276 <sup>a</sup> 241 <sup>b</sup>	30 °C	[36]
3533	PTMO/PA12	70	30	204 <sup>a</sup> 256 <sup>b</sup>	30 °C	[36]
1657	PEO/PA12	60	40	66.5	25 °C	[11]
4011	PEO/PA6	57	43	109 <sup>a</sup> 71.4 <sup>b</sup>	30 °C	[36]
1074	PEO/PA12	55	45	94 <sup>a</sup> 106 <sup>b</sup>	30 °C	[36]
				110.7	25 °C	[37]
4033	PTMO/PA12	53	47	81 <sup>a</sup> 95 <sup>b</sup>	30 °C	[36]

PEO: polyethylene oxide; PTMO: polytetramethylene oxide; PA6: polyamide 6; PA11: polyamide 11; PA12: polyamide 12; <sup>a</sup> prepared using 1-butanol as solvent; <sup>b</sup> prepared using cyclohexanol as solvent.

### 3.1. Different Behaviour of the Two ILs

The decline in permeability, observed in the nanocomposites that encapsulate impermeable fillers, originates from more tortuous paths imposed on the permeating gas molecules and/or from filler/polymer interactions [42]. The ratio of the composite membrane permeability to that of the neat matrix ( $P/P_0$ ) decreases more in the membranes comprising 10% IL2. The presence of the oxygen ether atom in the alkyl side chain of the IL2 cation could be responsible for stronger interactions with the polymer, as inferred by the thermal analysis. Moreover, the smaller molecular weight of IL2 implies a larger number of moles and, thus, more ions are present in the IL2-loaded membrane samples at the same weight loading of ILs. In addition, its anion (PF<sub>6</sub>) is poorly nucleophilic and classified as a non-coordinating anion, resulting in a diminished anion–cation interaction that enables interactions with the polymer matrix. On the other hand, PEO polymers are capable of strongly interacting with ILs, promoting a cation–anion dissociation in the IL salt via O<sup>-</sup>–cation interactions [43]. Similar interactions can be expected for the prepared nanocomposite membranes in which the PTMO block is predominant, as indicated by the PTMO T<sub>g</sub> that is shifted at higher temperatures (Figure 6).

Typically, ILs bearing a longer alkyl side chain on the cation are characterized by a larger free volume amount [44]. This feature was detected in Imidazolium ILs with increasingly bulkier anions by Xenon NMR [45] and by Molecular Dynamics studies [46]. Molecular simulations showed larger voids in these ILs due to the reduced ion attraction [47]. A weak interionic interaction enables larger distances between ions, facilitating the insertion of CO<sub>2</sub> between these ions [47]. The bulkier anion in IL1 favors the ion displacement. Therefore, larger cages are expected in the neat IL1, counteracting the permeability depression due to the more rigid polymer matrix. However, at a high IL concentration (e.g., 20 wt%), the ILs hardly maintain the supramolecular assembly that characterizes the neat materials, and important permeability reductions can be observed.

The gas diffusion coefficient also evidences a clear decreasing trend upon the addition of ILs to Pebax compared to the pristine polymer matrix (Figure 9). The augmented cohesive energy density for the PTMO block in the nanocomposite films, indicated by its higher *T<sub>g</sub>*, hinders the gas diffusion.

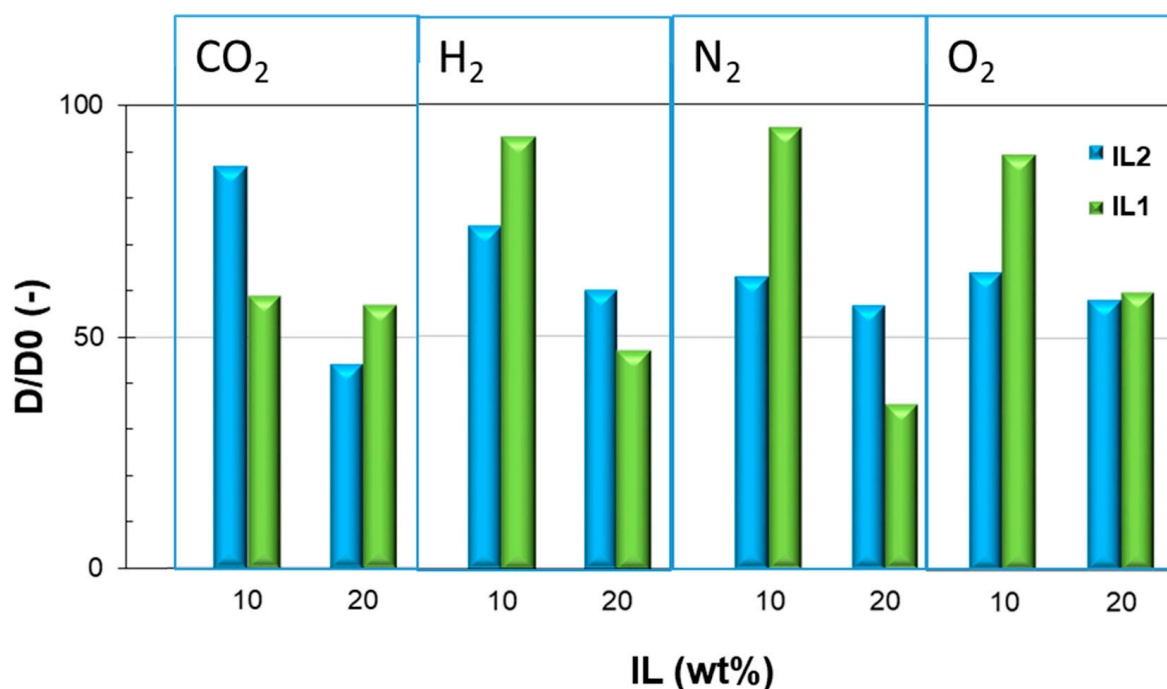


**Figure 9.** Gas diffusion coefficient in as-prepared Pebax<sup>®</sup>Rnew composite membranes relative to neat Pebax<sup>®</sup> ( $D/D_0$ ).  $T = 25\text{ }^\circ\text{C}$ .

### 3.2. Temperature Effect

The gas permeability through the Pebax membranes, as well as in all Pebax/ILs films, increased with temperature. However, gas sorption in polymers depends sensitively on temperature, and the predominant solubility contribution for CO<sub>2</sub> is depressed by increasing the temperature. Accordingly, a higher CO<sub>2</sub>/N<sub>2</sub> selectivity can be achieved in the Pebax matrix by reducing the operating temperature. Thus, the gas transport mechanism is diffusion-dominated in the temperature range tested.

The temperature-dependent permeation in the nanocomposite membranes differs from the neat copolymer, as shown in Figure 10, in the case of CO<sub>2</sub> for the blends loaded with 20% of ILs. Gas transport properties show a discontinuity at a temperature close to the melting point of the ILs (i.e., 50 °C as observed in the DSC trace). Below their melting point, the solid long chain ILs reduce the permeability of the polymer. Above this temperature ( $1000/T \approx 3.1\text{ K}^{-1}$ ), there is a jump in the gas permeability coefficient. A similar discontinuity was reported for the ionic conductivity of a piperidinium IL and attributed to the IL solid–liquid transition upon heating [43].

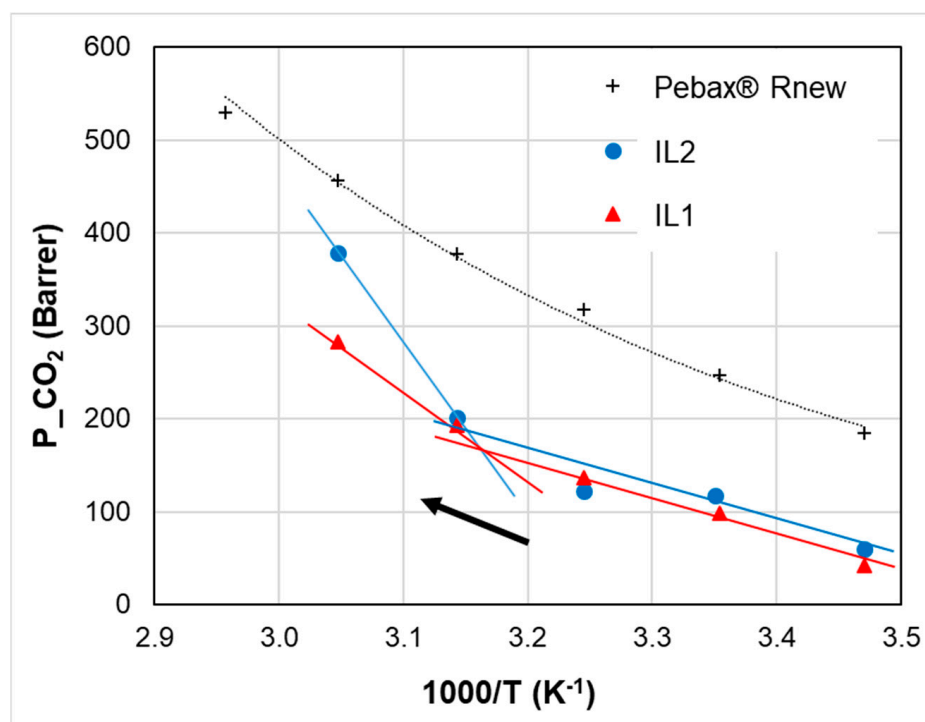


**Figure 10.** Temperature effect on CO<sub>2</sub> permeability for Pebax®Rnew and Pebax®Rnew–IL composite membranes at 20% of IL loading. Heating mode. Lines are a guide for the eyes.

Moreover, by changing the IL, different temperature-responsive behaviors can be established for the same copolymer (Figure 10). In particular, above the IL melting, IL2 is more efficient in increasing the gas permeability at higher temperatures.

An increased temperature substantially diminishes the intensity of intermolecular interactions, reducing the IL viscosity. Indeed, the viscosity is significantly enhanced in ILs with a large cation size. This is particularly evident in asymmetric cations [ $C_{N-1}C_1im$ ] above  $N = 6$ , due to the increase in the conformational entropy and the possibility of alkyl chain folding [48]. Thus, the considered ILs are highly viscous in the liquid state, reflecting the high molecular weight, as well as the intermolecular interactions (e.g., H-bonding, dispersive and electrostatic interactions), particularly IL1.

The temperature dependency of permeation parameters in the neat Pebax membrane can be approximated by an Arrhenius expression:

$$P = P^0 \exp(-E_p/RT) \quad (5)$$

where  $P^0$  is a pre-exponential factor and  $E_p$  is the apparent activation energy for permeation [49].

An Arrhenius behavior is observed above and below the IL melting point in the nanocomposite films. Thus, two activation energies were evaluated (Table 4). As stated for thermodynamic properties of ILs, in order to have reproducible data, they should be collected in heating modes [50]. Therefore, we took the data from heating scans to obtain the activation energies of the different samples.

The  $E_p$  values in the nanocomposite membranes are higher than in the neat Pebax film (Table 3), indicating their more pronounced sensitivity with respect to temperature changes, but also a denser structure.

In all prepared films, the order of  $E_p$  was:  $N_2 > O_2 > H_2 \approx He > CO_2$  (Table 3), showing the greatest influence of temperature on the less permeable species (e.g.,  $N_2$ ). Accordingly, the permselectivity for large/small gas pairs is generally depressed by increasing the temperature because the less permeable species present a higher activation energy than more permeable molecules.

**Table 4.** Apparent activation energy for permeation ( $E_p$ ), evaluated in the temperature range of 15–55 °C, for Pebax®Rnew films and representative Pebax/ILs samples.  $E_{p1}$  below the IL  $T_m$ ;  $E_{p2}$  above the IL  $T_m$ .

Sample		Activation Energy for Permeability ( $\text{kJ mol}^{-1}$ )			
		CO <sub>2</sub>	O <sub>2</sub>	N <sub>2</sub>	H <sub>2</sub>
Neat Rnew	$E_p$	17.0	28.0	32.7	26.7
Rnew-10% IL2	$E_{p1}$	22.8	34.6	42.3	27.3
	$E_{p2}$	38.0	50.4	53.6	41.4
Rnew-20% IL2	$E_{p1}$	26.0	37.2	42.3	34.1
	$E_{p2}$	47.6	55.3	62.2	45.3
Rnew-10% IL1	$E_{p1}$	18.8	29.0	37.1	19.1
	$E_{p2}$	19.9	33.9	40.6	30.2
Rnew-20% IL1	$E_{p1}$	43.3	49.7	59.6	35.6
	$E_{p2}$	30.5	42.9	46.6	46.3

At a concentration of 10%, the smaller IL2 induces significant changes in the  $E_p$  in the whole range of investigated temperatures, whereas the bulkier IL1 does not evidence significant differences with respect to the neat polymer. This is consistent with the polymer/IL interactions that are expected to be more significant in the molten state for IL2, which brings the ether oxygen on the cation side chain, as also evidenced by the DSC and TGA analysis. At a loading of 20%,  $E_{p2}$  remains still higher for IL2 for all the tested gas species, while  $E_{p1}$  becomes higher for films incorporating IL1.

### 3.3. Thermal Cycling

To examine the thermal response of the fabricated membranes, the operating temperature was changed in a cyclic way during the permeation tests, considering ranges that include the IL liquid–solid transition temperature ( $T_m$ ). A different temperature sensitivity in the nanocomposites was demonstrated with respect to pristine Pebax membranes.

A permeability hysteresis was established for CO<sub>2</sub>, as shown by also recording the permeation fluxes during the cooling in a temperature range that included the IL  $T_m$ . Figure 11 describes the behavior of the sample loaded with 10% IL2 upon heating and cooling that was carried out with comparable heating and cooling rates.

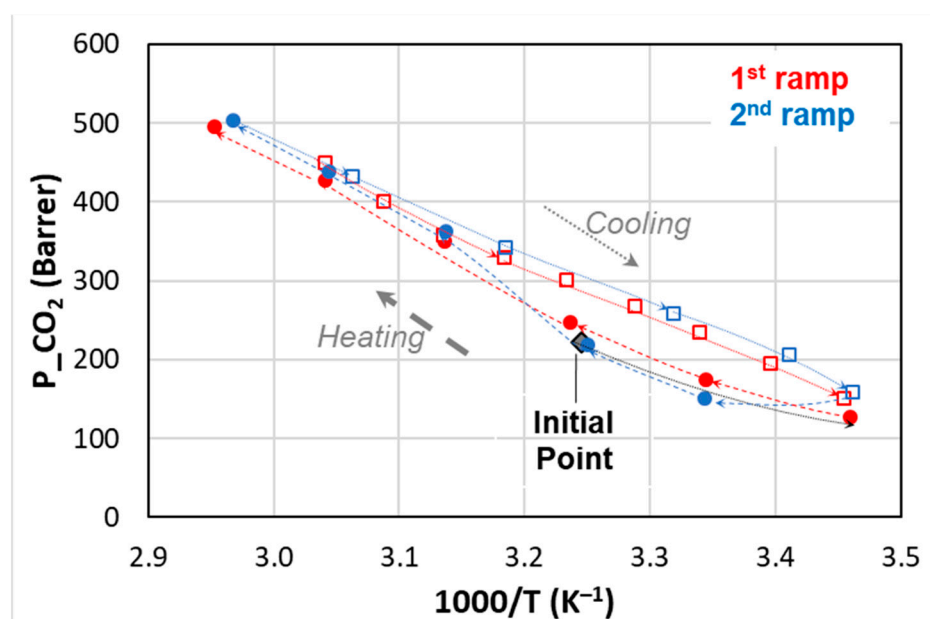


**Figure 11.** Temperature effect on CO<sub>2</sub> permeability for Rnew-10% IL2 composite membrane. Closed symbols: heating; open symbols: cooling.

Starting from the solid state of the IL ( $T = 35\text{ }^{\circ}\text{C}$ ), the membrane was first cooled at  $15\text{ }^{\circ}\text{C}$  and then its permeability was measured by increasing the temperature. No permeability hysteresis was found when the changes were below the IL  $T_m$ .

Upon heating, the  $\text{CO}_2$  permeability increases forming a knee: a low slope below the IL  $T_m$  and a steeper behavior above IL  $T_m$ . Instead, upon cooling from a temperature  $> T_m$ , the permeability decay was quite linear in the plot  $P$  vs.  $1/T$ , and the experimental points were located above those measured in the heating ramp. Thus, the film was more permeable in the  $T$  range below the melting of the IL when the low  $T$  was reached from the melt state of the IL.

The data are reproducible when repeated heating and cooling ramps are carried out.

However, the membrane microstructure reached upon cooling allows the permeation of small gases that experience a lower resistance than larger molecules. Indeed, no hysteresis is observed as far as small gas molecules are considered (e.g., He and  $\text{H}_2$ ) since the permeability curves in the first and second heating ramp are quite similar (Figure 12). Thus, the selectivity of the membrane can be changed depending on the heating or cooling.

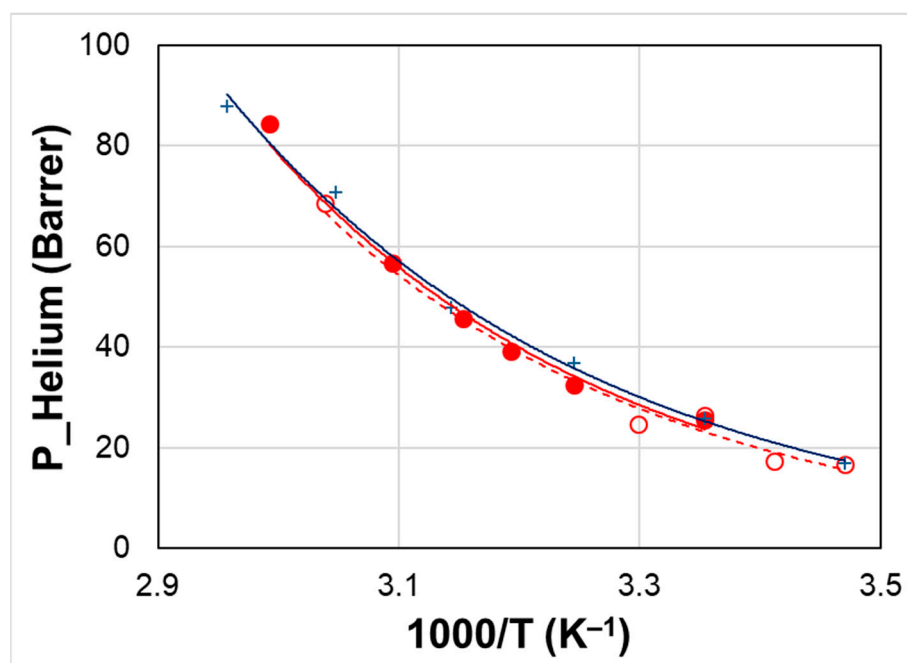


**Figure 12.** Temperature effect on Helium permeability for Rnew (plus sign, +) and Rnew-10% IL1 (HdmimDMSIP) composite membranes (circle). Closed symbols: heating; open symbols: cooling.

Other tests carried out with  $\text{CO}_2$  showed more significant hysteresis, as evidenced for the sample containing 10% IL2 and attaining permeability values very close to those of the neat polymer upon rapid cooling (Figure 13). A comparison is presented with the film containing 20% IL2 performing the cooling below the IL  $T_m$ , from  $45$  to  $25\text{ }^{\circ}\text{C}$ .

These tests (Figures 11 and 13) show that the rate of the temperature change affects the material response. Indeed, ILs can display complex thermal behavior owing to their nanostructuration, which is determined by charge neutrality constraints and the segregation of their non-polar long alkyl chains [50]. Compared from atomic and molecular liquids, ILs present an internal degree of freedom, permitting conformational changes with  $T$  [51]. However, solidification kinetics are commonly slow for ILs. Accordingly, a high rate in the  $T$  variation prevents the gel membrane from returning to its initial structure, remaining quite permeable. On the contrary, a different behavior can be established by keeping the composite samples at low  $T$  for long equilibration times, as evidenced by the low permeability values (Figure 12). Indeed, upon cooling from the liquid state, the ILs may form a glass at a low temperature [50].

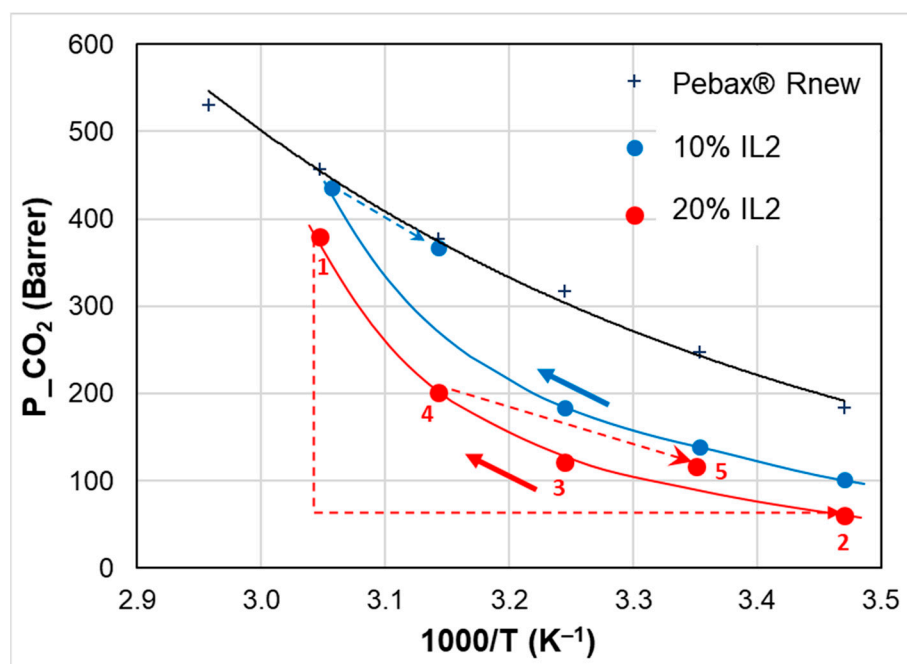


Figure 13. Temperature effect on CO<sub>2</sub> permeability for Rnew (plus sign, +) and Rnew–IL2 (OOMmimPF<sub>6</sub>) composite membranes at 20% (red circles) and 10% IL (blue circles).

Figure 14 shows the response to repeated temperature cycles of the membrane containing 10% IL1, recording the data during the heating ramps, performed at different rates.

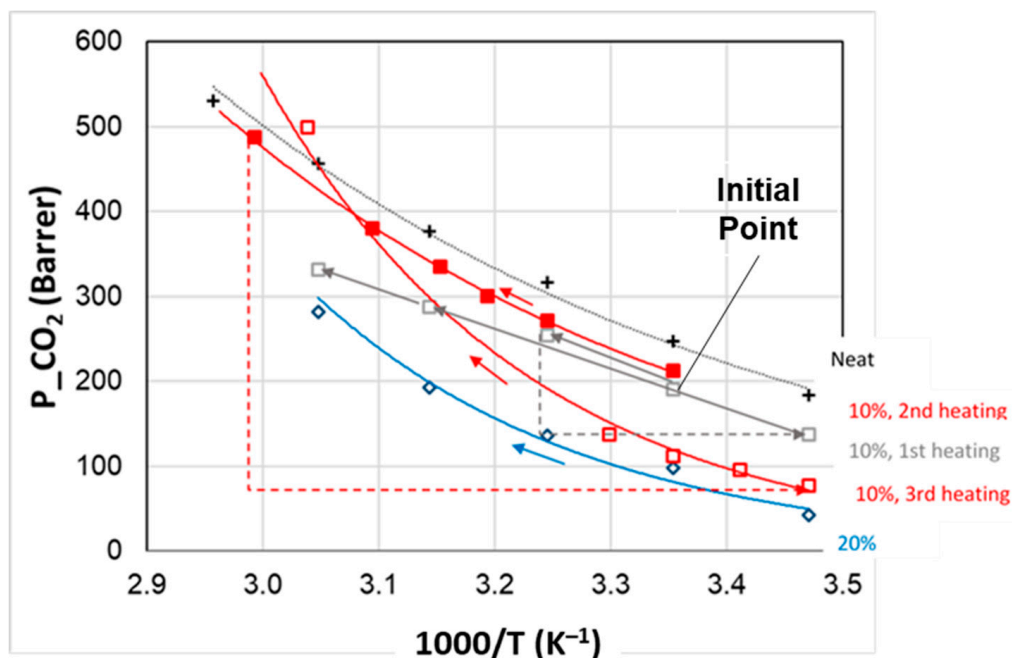


Figure 14. CO<sub>2</sub> permeability measured during heating ramps in Rnew–10% IL1 composite membrane compared to neat Rnew and Rnew–20% IL2 composite membrane. Lines are the exponential fit of the experimental points.

The CO<sub>2</sub> permeability measured on the as-prepared membrane in the first heating cycle (from 25 to 35 °C, then cooling at 15 °C and heating up to 45 and 55 °C) was quite below the value of the neat polymer, reflecting a more impermeable structure.

In a second heating cycle (from 25 to 60 °C), the permeability values at 25 and 35 °C were confirmed, while at a higher temperature, the permeation fluxes were larger and closer to those measured for the neat Pebax. Indeed, this ramp was carried out by taking more measurements and, thus, the changes are gradual and allow an equilibration of the sample at each temperature after small variations. After cooling from 60 to 15 °C and keeping the temperature low overnight, during the third heating, the sample presented a quite low permeability in the range 15–30 °C, close to the data obtained for the membrane containing 20% IL1. In this case, the microstructure of the sample was rearranged in a different way with respect to the as-prepared sample. Indeed, upon a slow cooling from 65 to 15 °C, with a prolonged time at low temperature, a denser structure with a redistribution of gaps was obtained. Instead, the membranes were obtained. As also evidenced by DSC traces recorded during heating and cooling, the as-prepared film, formed after the slow solvent evaporation of a solution that was magnetically stirred, reaching a certain dispersion of the IL, and used for the first heating cycle, behaved differently compared to the same film upon cooling from a melt IL state.

However, the high permeability can be recovered by the slow heating of the composite sample from 30 to 55 °C. Indeed, once above the IL  $T_m$ , the gas permeability evaluated at 55 °C surpassed the neat polymer line. This demonstrates how the rate of the thermal changes has a relevant role in the temperature-responsive behavior of the developed composites that are based on the combination of a rubbery polymer and ILs with a low solid–liquid temperature.

#### 4. Conclusions

Temperature-responsive composite membranes were prepared via the solution casting technique, incorporating two synthesized ILs (IL1, HdmimDMSIP and IL2, OOMmimPF<sub>6</sub>) within a rubbery polymer matrix of Pebax®Rnew, based on a bio-polyamide. The ILs present the Imidazolium group with long alkyl side chains on the cation and are solid at room temperature (solid–liquid transition around 50 °C). Both the polymer matrix and the selected ILs are interesting for separating polar and non-polar gas pairs.

The salts have a barrier effect on the gas permeation and a permeability decline is observed for the as-prepared nanocomposites. The performance of the nanocomposite films can be modulated by changing the IL type and its amount. A thermal analysis of the nanocomposite membranes indicates a somewhat reduced thermal stability upon the loading of the ILs and a complexation of IL2, having an oxygen in the alkyl side chain of the cation with the polymer matrix. The two blocks are differently affected by the ILs. FT-IR proves that the added ILs interact with the PA block in the copolymer matrix. The melting temperature for the crystalline part of the PA block is reduced upon the IL loading, while the glass transition temperature for the predominant soft PTMO block increases.

Gas permeation evidences a temperature-responsive behavior in the films loaded with both ILs, with a discontinuity as the temperature approached the IL structural transition. The temperature dependence for the gas permeability follows an Arrhenius-type thermally-activated behavior with two activation energies, below and above the melting of the IL.

Differently from small molecules such as He and H<sub>2</sub>, permeability hysteresis can be found for large and soluble molecules such as CO<sub>2</sub>, due to temperature-responsive changes in the membrane microscopic morphology that originate from the hierarchical structure of the ILs and the presence of long alkyl chains in the ILs. However, no defects are evident at a low temperature, at which the ILs are in a solid state upon the repeated thermal cycles. Interestingly, the temperature response of the gas transport through the prepared polymer gel/ILs composite membranes can be tailored by simply changing the rate of the temperature variations across the IL solid–liquid transition.

**Author Contributions:** Conceptualization, P.B. and G.C.; methodology, P.B.; formal analysis, D.C.Z. and P.B.; investigation, G.C. and D.C.Z.; resources, P.B., G.C. and D.C.Z.; data curation, G.C. and D.C.Z.; writing—original draft preparation, P.B.; writing—review and editing, P.B., G.C. and D.C.Z.;

visualization, P.B. and D.C.Z.; supervision, P.B.; project administration, P.B.; funding acquisition, P.B. All authors have read and agreed to the published version of the manuscript.

**Funding:** The project Prin 2017 “MultiFunctional polymer cOmposites based on groWn matERials (MIFLOWER)” (grant number: 2017B7MMJ5\_001) from the Italian Ministry of Education and University is kindly acknowledged.

**Institutional Review Board Statement:** Not applicable.

**Data Availability Statement:** Data presented in this study are available on request from the corresponding author.

**Acknowledgments:** Arkema Italy is gratefully acknowledged for providing the Pebax®Rnew samples.

**Conflicts of Interest:** The authors declare no conflict of interest.

## References

1. Adibfar, A.; Hosseini, S.; Eslaminejad, M.B. Smart Polymeric Systems: A Biomedical Viewpoint. In *Cell Biology and Translational Medicine, Volume 10*; Advances in Experimental Medicine and Biology; Turksen, K., Ed.; Springer: Cham, Switzerland, 2020; Volume 1298.
2. Hoogenboom, R. Chapter 2—Temperature-responsive polymers: Properties, synthesis and applications. In *Smart Polymers and Their Applications*; Elsevier: Amsterdam, The Netherlands, 2014; pp. 15–44.
3. Zhu, J.; Bai, L.; Chen, B.; Fei, W. Thermodynamical properties of phase change materials based on ionic liquids. *Chem. Eng. J.* **2009**, *147*, 58–62. [[CrossRef](#)]
4. Todros, S.; Natali, A.N.; Piga, M.; Giffin, G.A.; Pace, G.; Noto, V.D. Interplay between chemical structure and ageing on mechanical and electric relaxations in poly(ether-block-amide)s. *Polym. Degrad. Stabil.* **2013**, *98*, 1126–1137. [[CrossRef](#)]
5. Cai, J.; Jiang, J.; Zhou, Z.; Ding, Y.; Zhang, Y.; Wang, F.; Han, C.; Guo, J.; Shao, Q.; Du, H.; et al. Toughening Poly(lactic acid) by Melt Blending with Poly(ether-block-amide) Copolymer. *Sci. Adv. Mater.* **2017**, *9*, 1683–1692. [[CrossRef](#)]
6. Bondar, V.; Freeman, B.D.; Pinnau, I. Gas transport properties of poly(ether-b-amide) segmented block copolymers. *J. Polym. Sci. Part B Polym. Phys.* **2000**, *38*, 2051–2062. [[CrossRef](#)]
7. Bernardo, P.; Jansen, J.C.; Bazzarelli, F.; Tasselli, F.; Fuoco, A.; Friess, K.; Izák, P.; Jarmarová, V.; Kačirková, M.; Clarizia, G. Gas transport properties of PEBAX®/Room Temperature Ionic Liquid gel membranes. *Sep. Purif. Tech.* **2012**, *97*, 73–82. [[CrossRef](#)]
8. Magana, S.; Gain, O.; Gouanvé, F.; Espuche, E. Influence of different alkyl-methylimidazolium tetrafluoroborate ionic liquids on the structure of Pebax® films. Consequences on thermal, mechanical, and water sorption and diffusion properties. *J. Polym. Sci. Part B Polym. Phys.* **2016**, *54*, 811–824. [[CrossRef](#)]
9. Estahbanati, E.G.; Omidkhan, M.; Amooghin, A.E. Preparation and characterization of novel Ionic liquid/Pebax membranes for efficient CO<sub>2</sub>/light gases separation. *J. Ind. Eng. Chem.* **2017**, *51*, 77–89. [[CrossRef](#)]
10. Dong, L.-L.; Zhang, C.-F.; Zhang, Y.-Y.; Bai, Y.-X.; Gu, J.; Sun, Y.-P.; Chen, M.-Q. Improving CO<sub>2</sub>/N<sub>2</sub> separation performance using nonionic surfactant Tween containing polymeric gel membranes. *RSC Adv.* **2015**, *5*, 4947–4957. [[CrossRef](#)]
11. Bernardo, P.; Clarizia, G. Enhancing Gas Permeation Properties of Pebax® 1657 Membranes via Polysorbate Nonionic Surfactants Doping. *Polymers* **2020**, *12*, 253. [[CrossRef](#)]
12. Fu, Q.; Wong, E.H.H.; Kim, J.; Scofield, J.M.P.; Gurr, P.A.; Kentish, S.E.; Qiao, G.G. The effect of soft nanoparticles morphologies on thin film composite membrane performance. *J. Mater. Chem. A* **2014**, *2*, 17751–17756. [[CrossRef](#)]
13. Nafisi, V.; Hägg, M.-B. Development of Nanocomposite Membranes Containing Modified Si Nanoparticles in PEBAX-2533 as a Block Copolymer and 6FDA-Durene Diamine as a Glassy Polymer. *ACS Appl. Mater. Interfaces* **2014**, *6*, 15643–15652. [[CrossRef](#)] [[PubMed](#)]
14. Huang, G.; Isfahani, A.P.; Muchtar, A.; Sakurai, K.; Shrestha, B.B.; Qin, D.; Yamaguchi, D.; Sivaniah, E.; Ghalei, B. Pebax/ionic liquid modified graphene oxide mixed matrix membranes for enhanced CO<sub>2</sub> capture. *J. Membr. Sci.* **2018**, *565*, 370–379. [[CrossRef](#)]
15. Li, M.; Zhang, X.; Zeng, S.; Bai, L.; Gao, H.; Deng, J.; Yang, Q.; Zhang, S. Pebax-based composite membranes with high gas transport properties enhanced by ionic liquids for CO<sub>2</sub> separation. *RSC Adv.* **2017**, *7*, 6422–6431. [[CrossRef](#)]
16. Abdul Halim, K.A.; Kennedy, J.E.; Farrell, J.B. Preparation and Characterisation of Polyamide Homopolymer and Block Copolymer Nanocomposites. *Aust. J. Basic Appl. Sci.* **2013**, *7*, 108–115.
17. Cao, Y.; Mu, T. Comprehensive Investigation on the Thermal Stability of 66 Ionic Liquids by Thermogravimetric Analysis. *Ind. Eng. Chem. Res.* **2014**, *53*, 8651–8664. [[CrossRef](#)]
18. Capello, C.; Fischer, U.; Hungerbühler, K. What is a green solvent? A comprehensive framework for the environmental assessment of solvents. *Green Chem.* **2007**, *9*, 927–934. [[CrossRef](#)]
19. Otaegi, I.; Aranburu, N.; Guerrica-Echevarría, G. Attaining Toughness and Reduced Electrical Percolation Thresholds in Bio-Based PA410 by Combined Addition of Bio-Based Thermoplastic Elastomers and CNTs. *Polymers* **2021**, *13*, 3420. [[CrossRef](#)] [[PubMed](#)]
20. Clarizia, G.; Bernardo, P.; Carroccio, S.C.; Ussia, M.; Restuccia, C.; Parafati, L.; Calarco, A.; Zampino, D. Heterogenized Imidazolium-based ionic liquids in Pebax®RNew. Thermal, Gas transport and antimicrobial properties. *Polymers* **2020**, *12*, 1419. [[CrossRef](#)] [[PubMed](#)]

21. Zampino, D.; Mancuso, M.; Zaccone, R.; Ferreri, T.; Borzacchiello, A.; Zeppetelli, S.; Dattilo, S.; Ussia, M.; Ferreri, L.; Carbone, D.C.; et al. Thermo-mechanical, antimicrobial and biocompatible properties of PVC blends based on imidazolium ionic liquids. *Mater. Sci. Eng. C* **2021**, *122*, 111920. [[CrossRef](#)] [[PubMed](#)]
22. Clarizia, G.; Bernardo, P.; Gorrasi, G.; Zampino, D.; Carroccio, S.C. Influence of the preparation method and photo-oxidation treatment on the thermal and gas transport properties of dense films based on a poly(ether-block-amide) copolymer. *Materials* **2018**, *11*, 1326. [[CrossRef](#)] [[PubMed](#)]
23. Crank, J. *The Mathematics of Diffusion*, 2nd ed.; Clarendon Press: Oxford, UK, 1975.
24. Wijmans, J.G.; Baker, R.W. The solution-diffusion model: A review. *J. Membr. Sci.* **1995**, *107*, 1–21. [[CrossRef](#)]
25. Beiragh, H.H.; Omidkhan, M.; Abedini, R.; Khosravi, T.; Pakseresht, S. Synthesis and characterization of poly (ether-block-amide) mixed matrix membranes incorporated by nanoporous ZSM-5 particles for CO<sub>2</sub>/CH<sub>4</sub> separation. *Asia-Pac. J. Chem. Eng.* **2016**, *11*, 522–532. [[CrossRef](#)]
26. Nayebi, R.; Tarigh, G.D.; Shemirani, F. Porous ionic liquid polymer: A reusable adsorbent with broad operating pH range for speciation of nitrate and nitrite. *Sci. Rep.* **2019**, *9*, 11130. [[CrossRef](#)] [[PubMed](#)]
27. Rajkumar, T.; Ranga Rao, G. Synthesis and characterization of hybrid molecular material prepared by ionic liquid and silicotungstic acid. *Mater. Chem. Phys.* **2008**, *112*, 853–857. [[CrossRef](#)]
28. Zheng, D.; Dong, L.; Huang, W.; Wu, X.; Nie, N. A review of imidazolium ionic liquids research and development towards working pair of absorption cycle. *Renew. Sustain. Energy Rev.* **2014**, *37*, 47–68. [[CrossRef](#)]
29. Zoppi, R.A.; de Castro, C.R.; Yoshida, I.V.P.; Nunes, S.P. Hybrids of SiO<sub>2</sub> and poly(amide 6-b-ethylene oxide). *Polymer* **1997**, *38*, 5705–5712. [[CrossRef](#)]
30. Villanueva, M.; Coronas, A.; García, J.; Salgado, J. Thermal Stability of Ionic Liquids for Their Application as New Absorbents. *Ind. Eng. Chem. Res.* **2013**, *52*, 15718–15727. [[CrossRef](#)]
31. Shalu, S.K.; Chaurasia, R.K.; Singh, S. Chandra, thermal stability, complexing behavior, and ionic transport of polymeric gel membranes based on polymer PVdF-HFP and ionic liquid, [BMIM][BF<sub>4</sub>]. *J. Phys. Chem. B* **2013**, *117*, 897–906. [[CrossRef](#)]
32. Ahmadi, A.; Haghbakhsh, R.; Raeissi, S.; Hemmati, V. A simple group contribution correlation for the prediction of ionic liquid heat capacities at different temperatures. *Fluid Phase Equilibria* **2015**, *403*, 95–103. [[CrossRef](#)]
33. Farahani, N.; Gharagheizi, F.; Mirkhani, S.A.; Tumba, K. A simple correlation for prediction of heat capacities of ionic liquids. *Fluid Phase Equilibria* **2013**, *337*, 73–82. [[CrossRef](#)]
34. Ioelovich, M. Relationships between Cohesive Energy, Glass Transition Temperature and Melting Point for Various Polymers. *Sci. Isr.—Technol. Advant.* **2021**, *23*, 139–146.
35. Bernardo, P.; Clarizia, G. A review of the recent progress in the development of Nanocomposites based on poly(ether-block-amide) copolymers as membranes for CO<sub>2</sub> separation. *Polymers* **2022**, *14*, 10.
36. Barbi, V.; Funari, S.S.; Gehrke, R.; Scharnagl, N.; Striebeck, N. SAXS and the Gas Transport in Polyether-block-polyamide Copolymer Membranes. *Macromolecules* **2003**, *36*, 749–758. [[CrossRef](#)]
37. Azizi, N.; Mohammadi, T.; Behbahani, R.M. Comparison of permeability performance of PEBAX-1074/TiO<sub>2</sub>, PEBAX-1074/SiO<sub>2</sub> and PEBAX-1074/Al<sub>2</sub>O<sub>3</sub> nanocomposite membranes for CO<sub>2</sub>/CH<sub>4</sub> separation. *Chem. Eng. Res. Des.* **2017**, *117*, 177–189. [[CrossRef](#)]
38. Holloczki, O.; Kelemen, Z.; Kęnczyl, L.; Szieberth, D.; Nyulaszi, L.; Stark, A.; Kirchner, B. Significant Cation Effects in Carbon Dioxide-Ionic Liquid Systems. *Chem. Phys. Chem.* **2013**, *14*, 315–320. [[CrossRef](#)]
39. Xiong, Y.-B.; Wang, H.; Wang, Y.-J.; Wang, R.-M. Novel imidazolium-based poly(ionic liquid)s: Preparation, characterization, and absorption of CO<sub>2</sub>. *Polym. Adv. Technol.* **2012**, *23*, 835–840. [[CrossRef](#)]
40. Cadena, C.; Anthony, J.L.; Shah, J.K.; Morrow, T.I.; Brennecke, J.F.; Maginn, E.J. Why is CO<sub>2</sub> So Soluble in Imidazolium-Based Ionic Liquids? *J. Am. Chem. Soc.* **2004**, *126*, 5300–5308. [[CrossRef](#)]
41. Pilato, L.A.; Litz, L.M.; Hargitay, B.; Osborne, R.C.; Farnham, A.G.; Kawakami, J.H.; Fritze, P.; McGrath, J. Polymers for permselective membrane gas separations. *Polym Prepr.* **1975**, *16*, 41–46.
42. Wolf, C.; Angellier-Coussy, H.; Gontard, N.; Doghieri, F.; Guillard, V. How the shape of fillers affects the barrier properties of polymer/non-porous particles nanocomposites: A review. *J. Membr. Sci.* **2018**, *556*, 393–418. [[CrossRef](#)]
43. Elamin, K.; Shojaat Hosseini, M.; Danyliv, O.; Martinelli, A.; Swenson, J. Conduction mechanism in polymeric membranes based on PEO or PVdF-HFP and containing a piperidinium ionic liquid. *Electrochim. Acta* **2019**, *299*, 979–986. [[CrossRef](#)]
44. Supasitmongkola, S.; Styring, P. High CO<sub>2</sub> solubility in ionic liquids and a tetraalkylammonium-based poly(ionic liquid). *Energy Environ. Sci.* **2010**, *3*, 1961–1972. [[CrossRef](#)]
45. Castiglione, F.; Simonutti, R.; Mauri, M.; Mele, A. Cage-Like Local Structure of Ionic Liquids Revealed by a <sup>129</sup>Xe Chemical Shift. *J. Phys. Chem. Lett.* **2013**, *4*, 1608–1612. [[CrossRef](#)] [[PubMed](#)]
46. Saielli, G.; Bagno, A.; Castiglione, F.; Simonutti, R.; Mauri, M.; Mele, A. Understanding Cage Effects in Imidazolium Ionic Liquids by <sup>129</sup>Xe NMR: MD Simulations and Relativistic DFT Calculations. *J. Phys. Chem. B* **2014**, *118*, 13963–13968. [[CrossRef](#)]
47. Klähn, M.; Seduraman, A. What Determines CO<sub>2</sub> Solubility in Ionic Liquids? A Molecular Simulation Study. *J. Phys. Chem. B* **2015**, *119*, 10066–10078. [[CrossRef](#)] [[PubMed](#)]
48. Rocha, M.A.A.; Neves, C.M.S.S.; Freire, M.G.; Russina, O.; Triolo, A.; Coutinho, J.A.P.; Santos, L.M.N.B.F. Alkylimidazolium Based Ionic Liquids: Impact of Cation Symmetry on Their Nanoscale Structural Organization. *J. Phys. Chem. B* **2013**, *117*, 10889–10897. [[CrossRef](#)] [[PubMed](#)]

49. Barrer, R.M.; Rideal, E.K. Permeation, Diffusion and Solution of Gases in Organic Polymers. *Trans. Faraday Soc.* **1939**, *35*, 628–656. [[CrossRef](#)]
50. Valderrama, J.O.; Campusano, R.A.; Rojas, R.E. Glass transition temperature of Ionic Liquids using molecular descriptors and artificial neural networks. *Comptes Rendus Chim.* **2017**, *20*, 573–584. [[CrossRef](#)]
51. Harris, M.A.; Kinsey, T.; Wagle, D.V.; Baker, G.A.; Sangoro, J. Evidence of a liquid-liquid transition in a glass-forming ionic liquid. *Proc. Natl. Acad. Sci. USA* **2021**, *118*, e2020878118. [[CrossRef](#)]

**Disclaimer/Publisher’s Note:** The statements, opinions and data contained in all publications are solely those of the individual author(s) and contributor(s) and not of MDPI and/or the editor(s). MDPI and/or the editor(s) disclaim responsibility for any injury to people or property resulting from any ideas, methods, instructions or products referred to in the content.